ION DYNAMICS IN AURORAL POTENTIAL STRUCTURES AND FORMATION OF ION CONIC DISTRIBUTION

A

THESIS

presented to the Faculty of the

University of Alaska in Partial Fulfillment

of the Requirements

for the Degree of

MASTER OF SCIENCE

by

Wei-hong Yang, B.S.

Fairbanks, Alaska

December 1981

ION DYNAMICS IN AURORAL POTENTIAL STRUCTURES
AND FORMATION OF ION CONIC DISTRIBUTION

RECOMMENDED:

Chairman, Advisory Committee

Head, Space Physics and
Atmospheric Sciences Program

Director, Division of Geosciences

APPROVED:

Vice Chancellor for Research and Advanced Study

December 12, 1981.
Date

ABSTRACT

This thesis is concerned with the problem of how the positive ions are energized by the two-dimensional potential structures along auroral field lines; these auroral potential structures are known to be responsible for accelerating electrons into the ionosphere to produce discrete auroras. A systematic numerical study of the test ion dynamics in auroral potential structures, either V-shaped or S-shaped, has been carried out. Transverse ion accelerations occur if the width of the auroral potential structure (L_x) is smaller than the ion gyroradius (ρ_i). This result shows that the conic distribution of upstreaming ions observed on auroral field lines can be generated by the same potential structures which produce the thin auroral arcs ($L_x \lesssim \rho_i$). This transverse acceleration mechanism operates more effectively on heavier ions, resulting in O^+ ions more energetic than H^+ ions as indicated by observations.

ACKNOWLEDGMENTS

This thesis was written under the helpful guidance of my Advisory Committee consisting of Dr.S.-I. Akasofu, Dr.J. Kan, Dr.L.C. Lee, Prof. D.W. Swift, and Dr.J.L. Morack. I specially thank my advisor, Dr.S.-I. Akasofu, Dr.J. Kan, and Dr.L.C. Lee for many helpful discussions and their constant assistance. I also wish to thank Dr.J. Wagner and Mr.P. Gray for helping me to master the particle trajectory program. I would like to thank my friends B.-H. Ahn and K. Hakamada for helping me to learn the basic knowledge of using the computer. I also would like to thank many scientists and my fellow graduate students of this institute for their warm friendship. I owe special thanks to Ms.Karen Flesher for her typing of this manuscript. This work was supported by a grant from the National Science Foundation, Atmosphere Sciences Section, ATM-81-15321.

TABLE OF CONTENTS

LIST OF FIGURES

1. Introduction

Intense fluxes of upward flowing H^+ and O^+ with energies in keV range are frequently observed with experiments on the S3-3 satellite in the auroral and polar region (Ghielmetti et al., 1978; Gorney et al., 1981). The observations indicate that the energetic upward-flowing ions are of ionospheric origin. The upward-flowing ion events are classified into beams and conics. The ion distributions of beams have peak fluxes along the magnetic field direction, and those of conics exhibit flux maxima that are not field aligned.

The observation of upflowing ion beams requires parallel acceleration below the satellite since the magnetic mirror force alone cannot convert enough perpendicular energy to parallel energy to produce a beam at S3-3 altitudes. Similarly, the existence of upward-flowing ions with conical pitch-angle distributions requires perpendicular ion acceleration at altitudes below the observation point. The parallel acceleration may be accounted for by parallel electric field. The perpendicular acceleration leading to conic distribution is a topic of current research.

Several mechanisms have been proposed for the perpendicular acceleration. The possibility of resonant wave-particle interactions between the upgoing thermal ions with a parallel energy of several eV and the observed electrostatic ion cyclotron waves in regions of downward aurora currents has been discussed by Dusenbery and Lyons (1981). A numerical simulation of ion conic distribution due to intense ion heating in the presence of hydrogen cyclotron

waves has been conducted recently by Okuda and Ashour-Abdalla (1981). The possibility of perpendicular acceleration of ions by interactions with a spatially confined perpendicular DC electric field has been suggested by Chiu and Newman (1981).

This thesis is a study of perpendicular accelerations of ions in auroral potential structures in a uniform magnetic field. The auroral potential structures deduced from observations are either V-shaped or S-shaped (Gurnett, 1972; Swift et al., 1976; Cattell et al., 1979) as shown in Figure 1. The width of the potential structure (L_x) can be inferred from the width of discrete auroras (Davis, 1978). For inverted V precipitations, $L_x >> \rho_i$ (Lin and Hoffman, 1979) where ρ_i is the ion gyroradius. For the auroral arcs, $L_x \lesssim \rho_i$ (Maggs and Davis, 1968). The field-aligned scale length L_z is found to be much greater than the Debye length (Mizera and Fennell, 1977; Sharp et al., 1979).

Our study is carried out in two parts. We first analyze the nonadiabatic particle trajectories by solving the equation of motion numerically for ions under different initial conditions in potential structures of different width L_x is less than the ion gyroradius ($L_x \lesssim \rho_i$). This result implies that ion conics can be produced by the same potential structures which produce the thin auroral arcs. We then provide a theoretical interpretation of this numerical result by a generalization of Cole's (1976) pioneer work to the two-dimensional auroral potential structures.

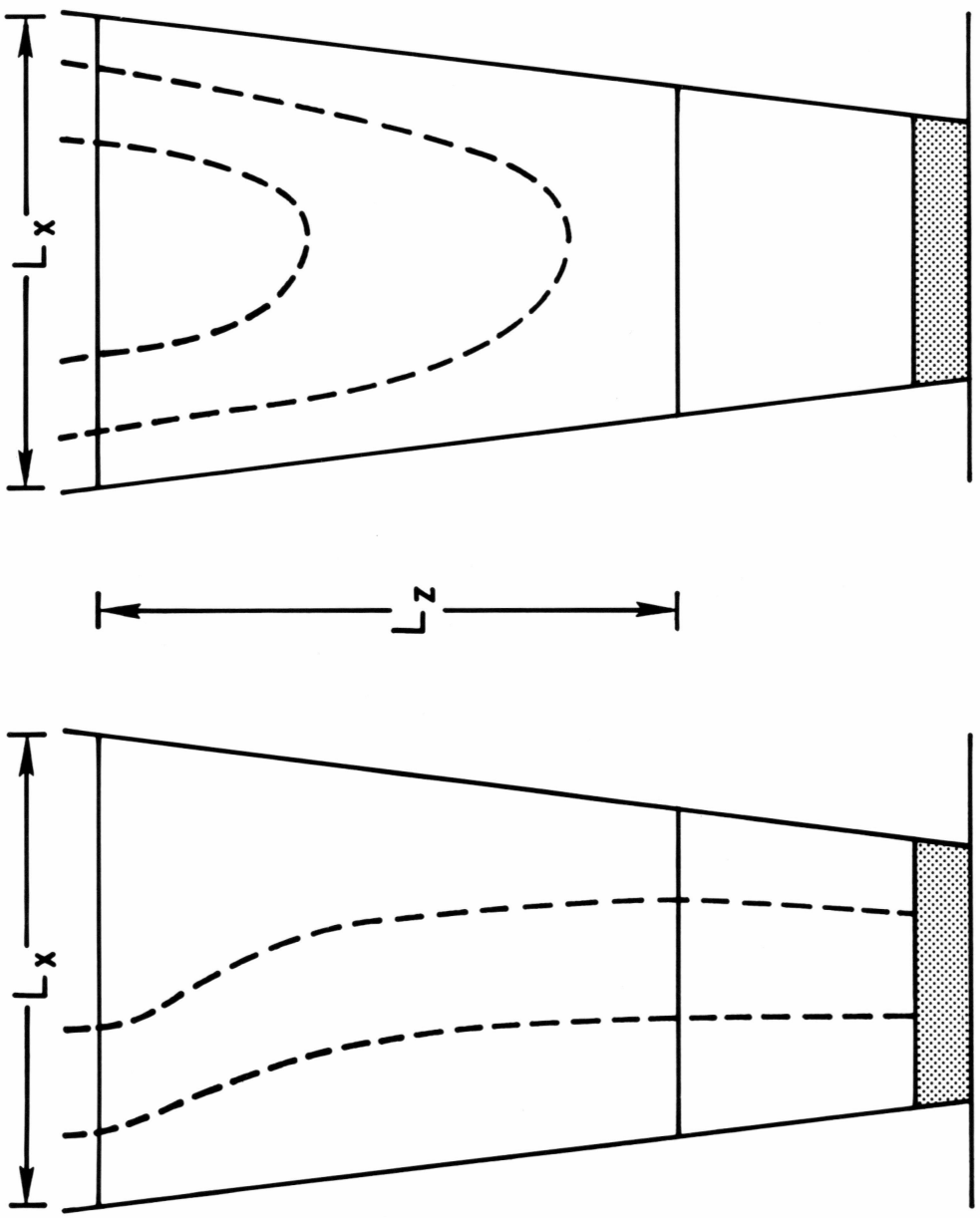

Figure 1.1 Schematic illustration of the S-shaped and V-shaped equipotential structures (dashed curve) along converging magnetic field lines.

2. A Survey of Observations

The S3-3 satellite was launched during the summer of 1976 into an elliptical polar orbit with an initial inclination of 97.5°, an apogee altitude of 8040 km, a perigee altitude of 240 km, and an orbital period of approximately three hours. The orbital plane drifted westward at a rate of about 1 hour of local time per 20 days, thus allowing complete local time coverage with a period of about 8 months. That the upflowing ions observed on S3-3 have an ionospheric origin has been shown by the data from the Lockheed experiment. The Lockheed experiment consisted of three ion mass spectrometers and four magnetic electron spectrometers. They were mounted with their view directions perpendicular to the spin axis. Once each spin period, the mass spectrometer looked down along the magnetic field line and measured the relative intensities of upflowing H^+, He^+, O^+.

2.1 Ion Beams

Figure 2.1.a, from Shelley et al. (1976), shows an example of upflowing ion beams observed with the low-energy ion spectrometer on July 13, 1976. The upper panel shows the pitch angle of the instrument view direction. Below it is indicated the energy per charge setting of the spectrometer. The spectrometer response to O^+ and H^+ ions is illustrated in the two center panels. The narrow field-aligned upward-flowing pitch-angle distributions are evident. The flux intensity corresponding to the peak response is

0.3×10^8 $(cm^2 \text{ sec ster keV})^{-1}$ for the 1.28 keV O^+ ions and 0.7×10^8 $(cm^2 \text{ sec ster keV})^{-1}$ for the 0.94 keV H^+ ions. The lowest panel shows electron fluxes in the energy range from 0.35 to 1.1 keV. The K_p value during the period of these observations was 2^-. Figure 2.1.b shows another example of ion beams observed on July 17, 1976. The K_p value for that period was 1. The narrow pitch-angle distributions aligned along the magnetic field direction are seen obviously from the figures.

2.2 Ion Conics

Examples of upflowing O^+ and H^+ ions exhibiting a conical pitch-angle distribution is illustrated in Figure 2.2, taken from Sharp et al. (1977). The top panel in this figure shows the O^+ data. The pitch-angle distribution of upflowing O^+ ions have a minimum along the magnetic field direction and a maxima in about the 130^o - 140^o range. The two bottom panels show the H^+ data for the lowest-energy spectrometers during the same period.

The pancake-like pitch-angle distribution of ionosphere ions at low altitude (~ 400 - 600 km) was observed from a rocket experiment (Whalen et al., 1978) in association with intense electron precipitation events. The data in Figure 2.3 show the observed ion pitch-angle distributions which sharply peak at the range 90^o - 120^o. Acceleration by ion cyclotron waves produced via a current-driven or beam-plasma instability was suggested as a possible source mechanism (Whalen et al., 1978).

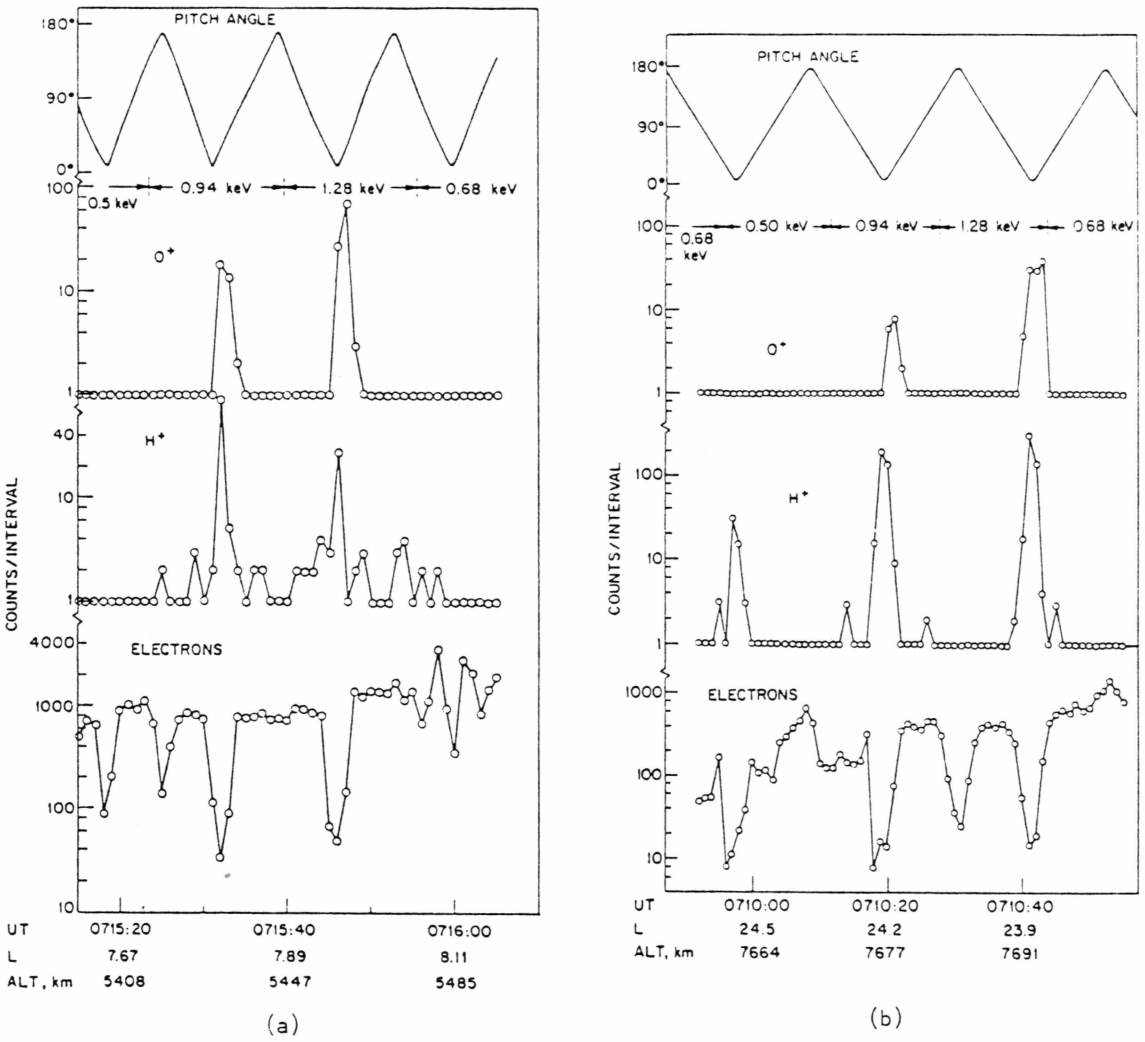

Figure 2.1 Upflowing ion beams observed from the S3-3 satellite in association with signatures of a parallel electric field in the electron data

(a) Data from Revolution 35 on July 13, 1976.

(b) Data from Revolution 67 on July 17, 1976.

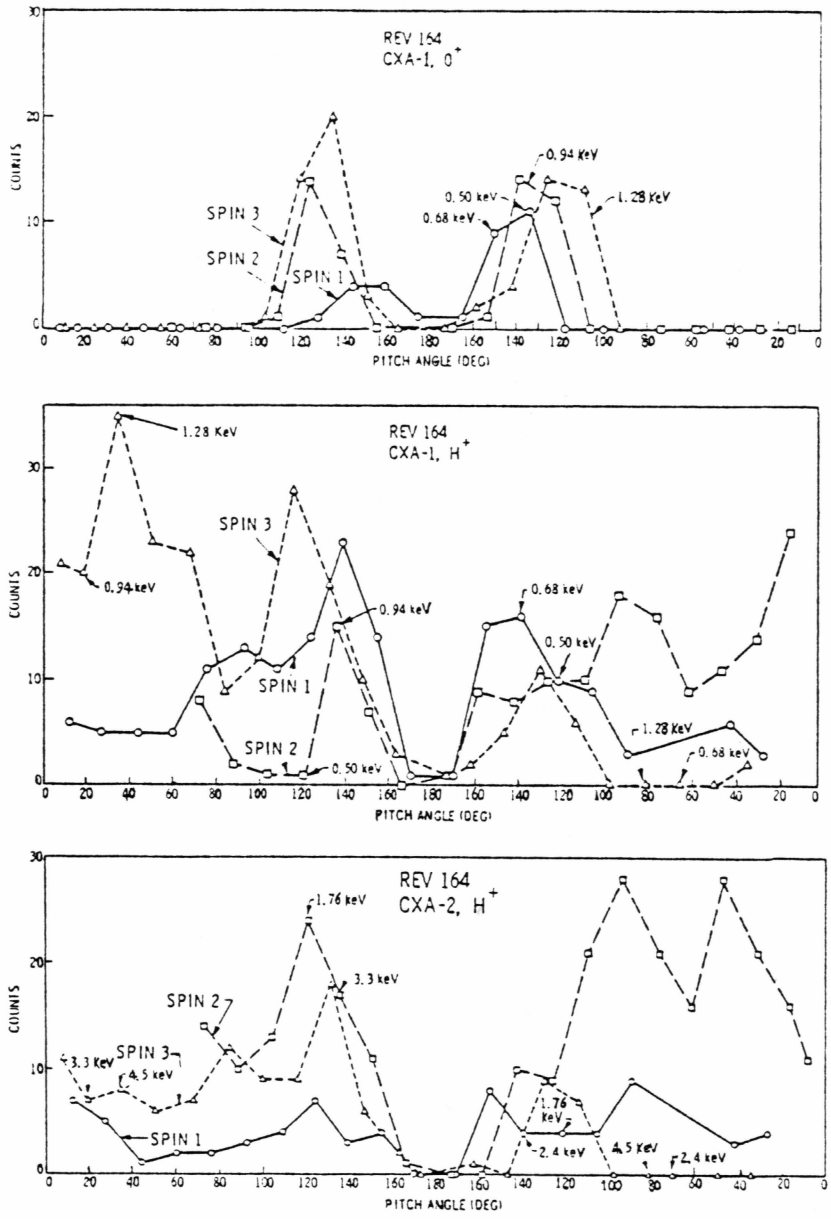

Figure 2.2 Ion data showing detailed pitch angle dependence of the low-energy O^+ and H^+ fluxes during the three spins of the 1976-65B satellite.

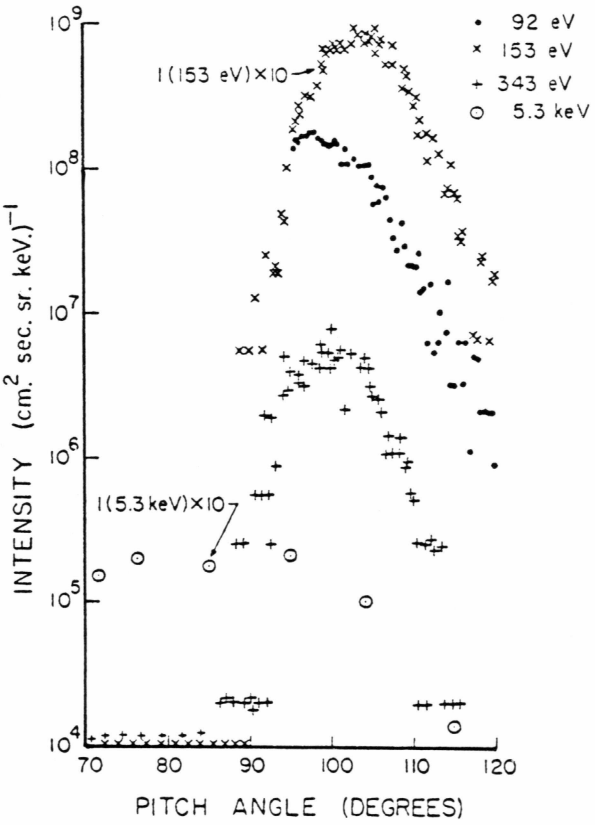

Figure 2.3 Ion pitch angle distributions observed by a Black Brant IVB (AAF-IVB-33) sounding rocket (Whalen et al., 1978).

2.3. Comparison of O^+ and H^+

Collin et al. (1980) have conducted a statistical study of O^+ and H^+ ion behaviors using the S3-3 data from the evening local time sector, at altitudes between 6000 and 8000 km during primarily quiet times. A scatter plot of the average energies of the simultaneously observed upward-flowing O^+ and H^+ ions is shown in Figure 2.4. The O^+ is seen to be systematically more energetic than the H^+. The ratio of their average energies for the data set shown was 1.7. The O^+ ions had significantly wider beam widths than the H^+ ions. A histogram of the occurrence probability versus half width (at half maximum) of the beams is shown in Figure 2.5. The median width of the O^+ ion peaks was 24^o and that of H^+ ions was 15^o.

3. Field Models

Self-consistent auroral potential models have been analyzed by several authors (Block, 1972; Kan, 1975; Swift, 1975, 1976, 1979; Kan et al., 1979; Chiu and Cornwall, 1980). For the purpose of studying test ion dynamics, we will use V-shaped and S-shaped potential structures which can be described by analytic expressions but need not be self-consistent solutions of the Vlasov-Poisson equations.

3.1. V-shape

The two-dimensional function of the V-shaped potential model is assumed to have the following expressions

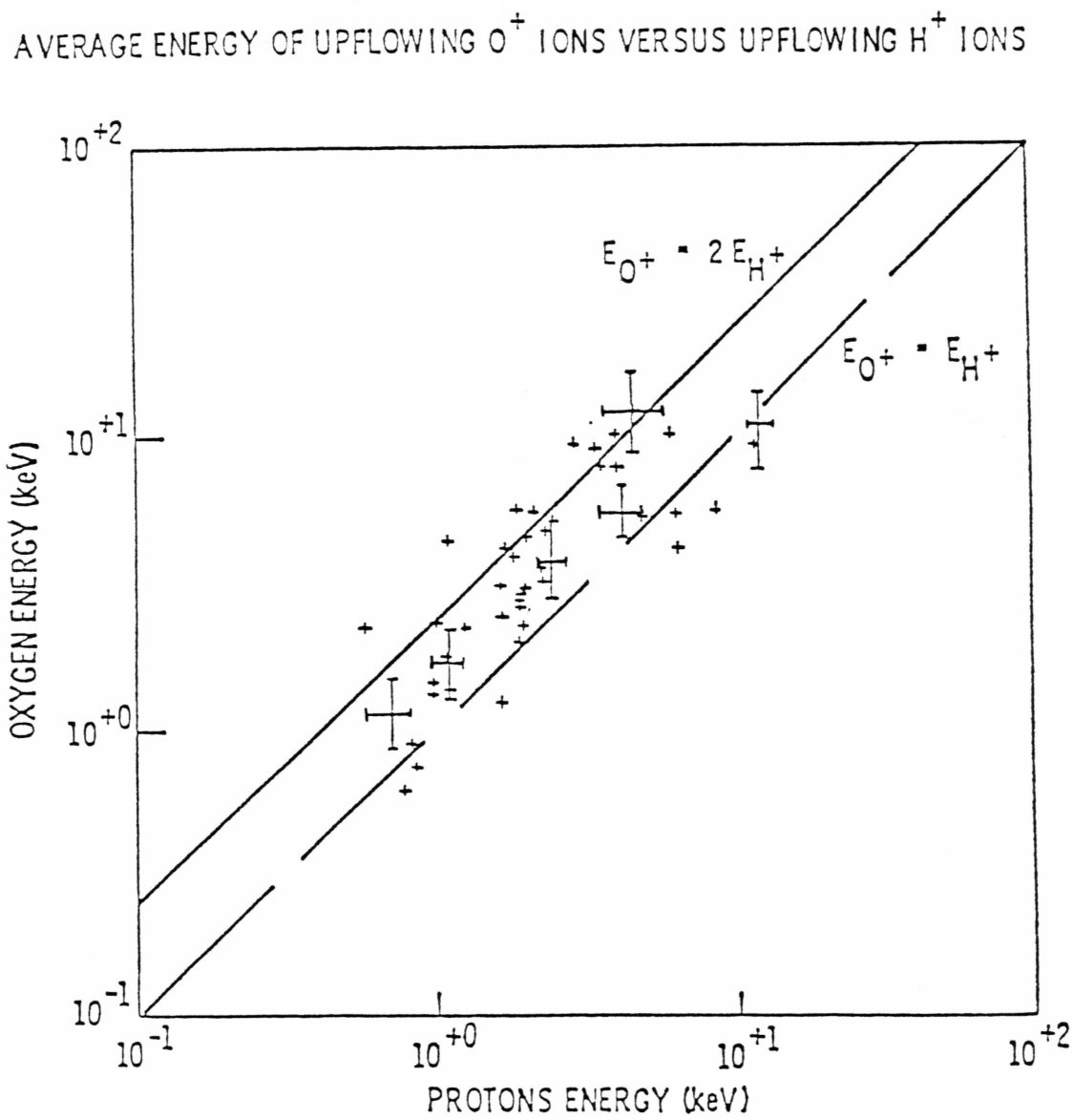

Figure 2.4 Scatter plot of average O^+ and H^+ energies in upflowing ion beams (Collins et al., 1980).

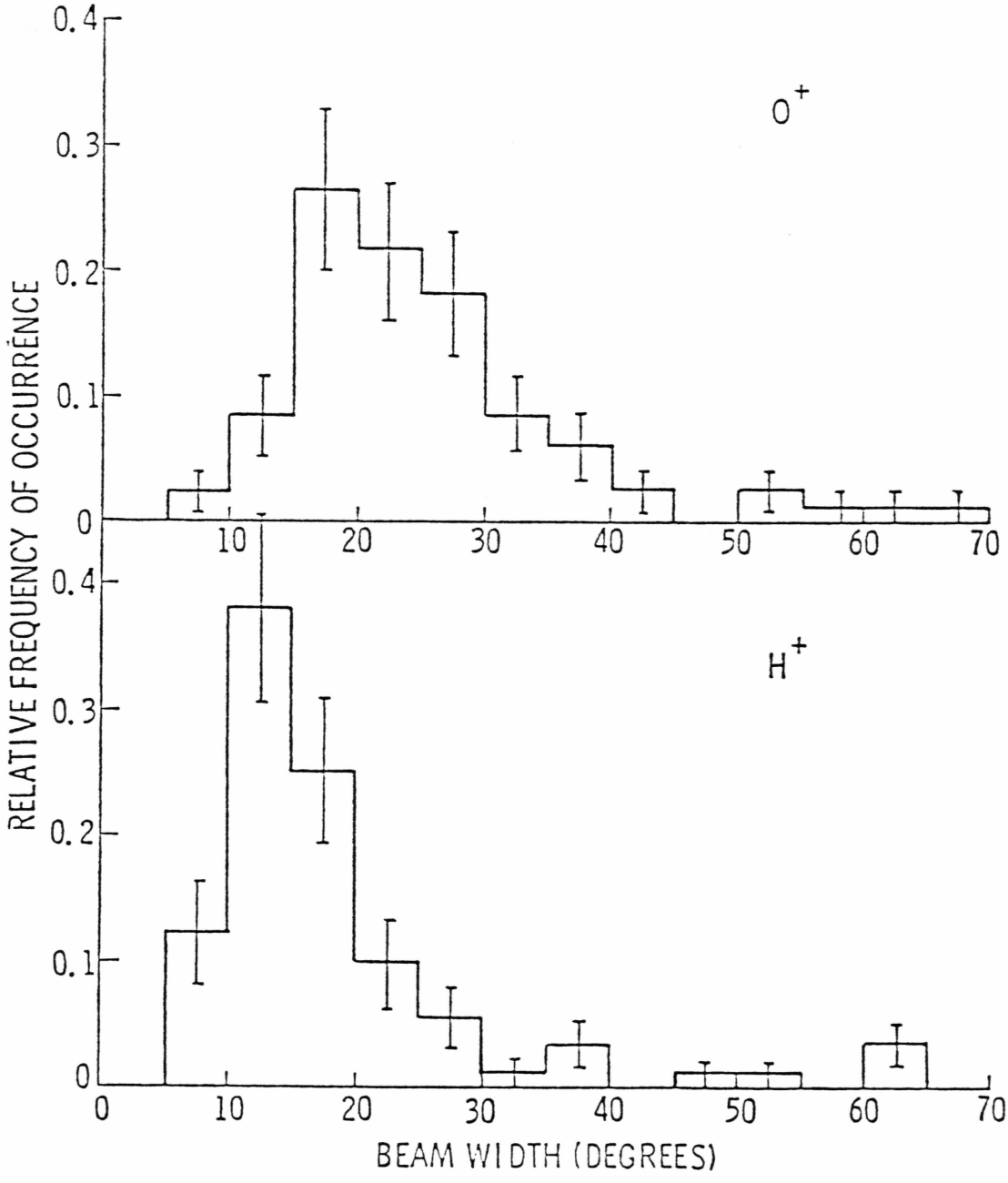

Figure 2.5 A comparison of the O^+ and H^+ beam widths from the upflowing ion events shown in Figure 2.4.

$$\phi(x,z) = \begin{cases} -\phi_o e^{-x^2/L_x^2}\left(1 - A \cdot e^{-z^2/L_z^2}\right), & z \geq 0 \\ -\phi_o (1 - A) e^{-x^2/L_x^2}, & z < 0 \end{cases} \tag{3.1}$$

where ϕ_o is the magnitude of the electric potential, L_x and L_z are characteristic scale lengths in the x and z directions; A is another characteristic constant, $0 \leq A \leq 1$. For A = 0, equation (3.1) gives a pure parallel equipotential structure; for A = 1, a pure V-shape equipotential structure is given; while $0 < A < 1$, the potential configuration is a pure V-shape with a pair of S-shaped wings. The configuration of the potential field is given by a set of values of A, L_x, and L_z; note L_x and L_z are in length unit.

Figure 3.1 exhibits the sample numerical results for the pure V-shaped potential (A = 1) in the x/L_x, z/L_z coordinate system. This figure gives us a general information about the spatial structure of the pure V-shaped electric potential.

Figure 3.2 shows an example of equipotential lines of a pure V-shaped potential with $L_x = 1.5$, $L_z = 20$, A = 1. Figure 3.3 shows a V-shaped potential configuration for $L_x = 1.5$, $L_z = 20.0$, and A = 0.8. Three regions may be distinguished in the structure; in region I, the V-shape potential acceleration dominates; in region II, the S-shape potential acceleration dominates, and in region III ($z < 0$),

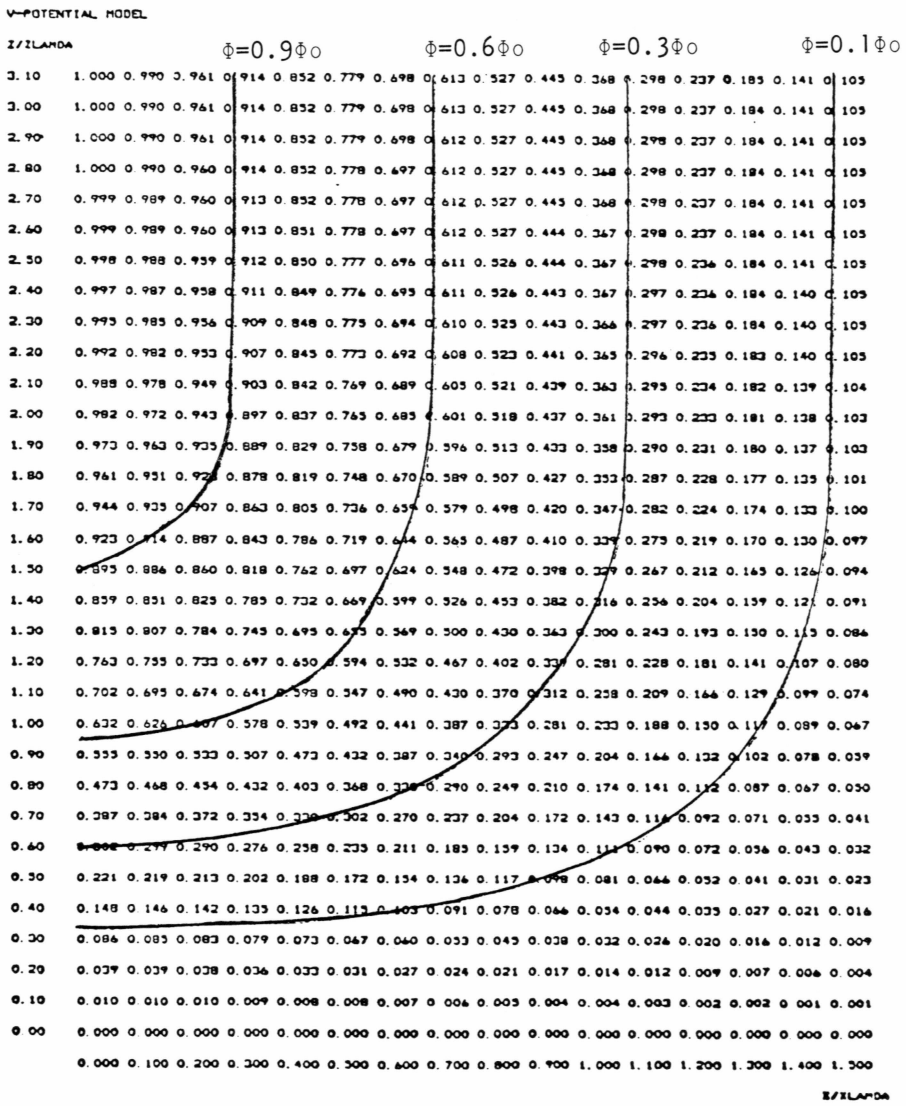

Figure 3.1 Sample numerical results for V-shaped potential structure in x/L_x, z/L_z coordinate system.

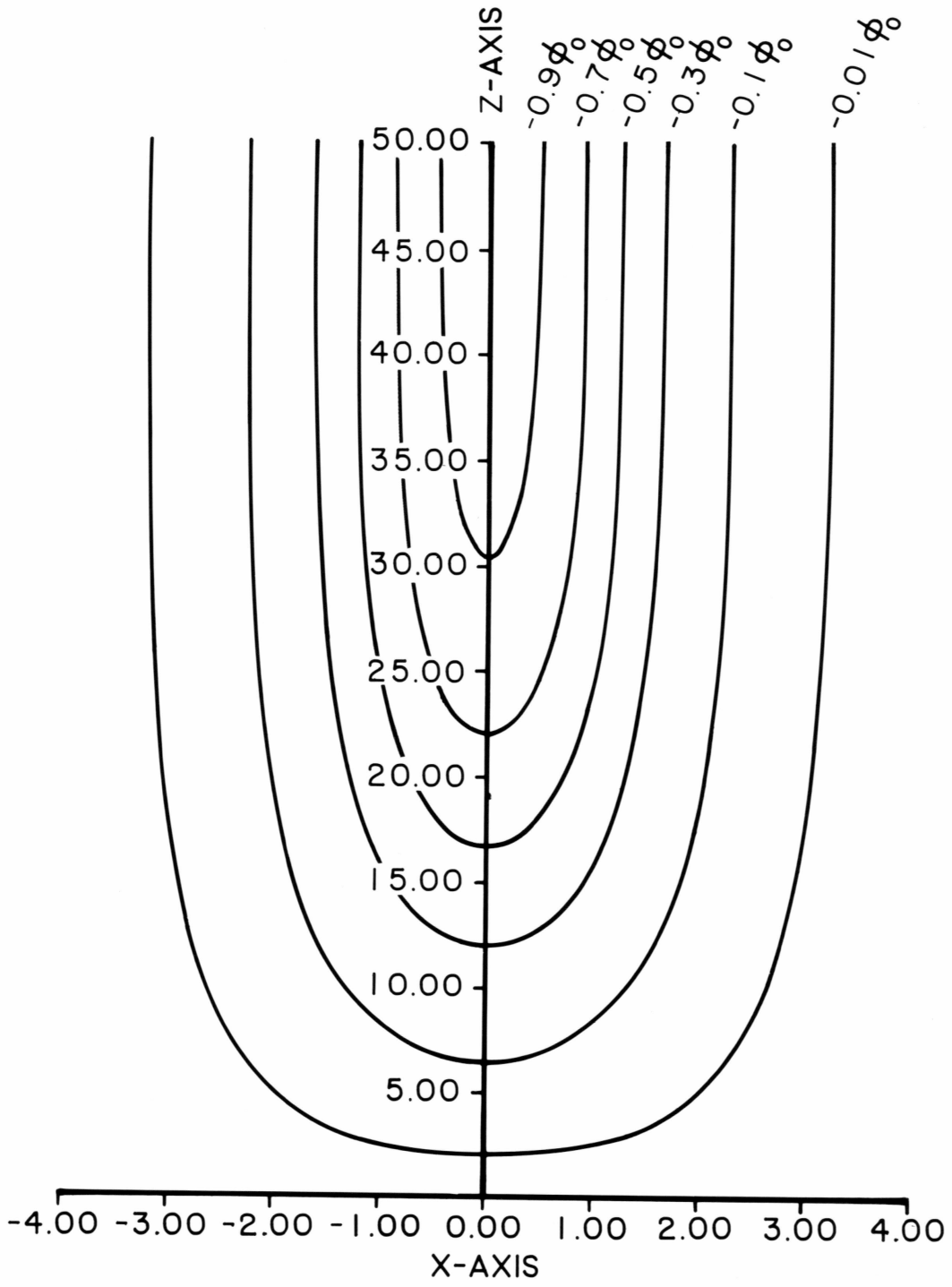

Figure 3.2 Illustration of a pure V-shaped equipotential struvture (L_x=1.5, L_z=20.0, A=1).

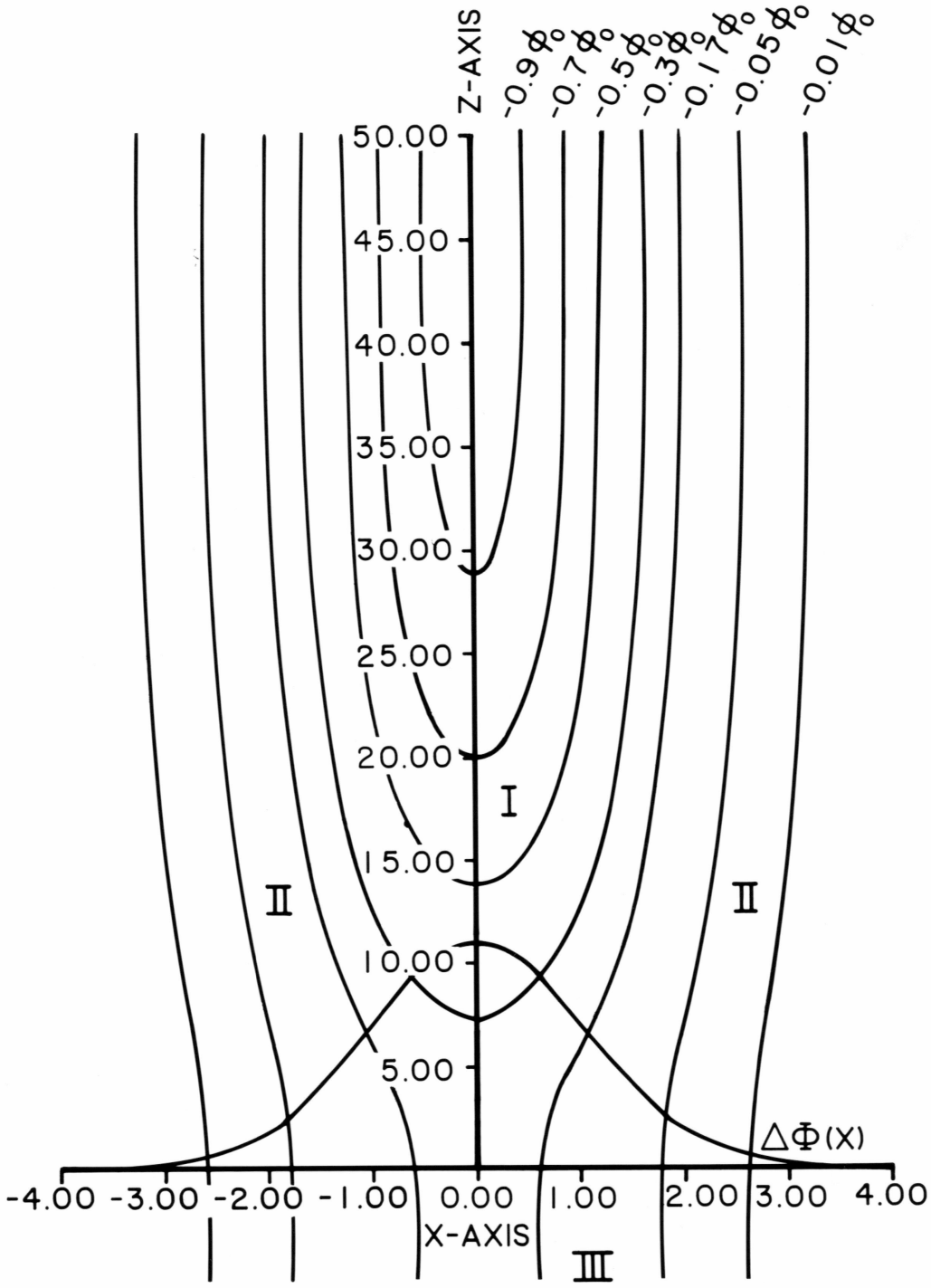

Figure 3.3 Illustration of a V-shaped equipotential structure (L_x=1.5, L_z=20.0, A=0.3).

the perpendicular electric field acceleration dominates.

From equation (3.1), when $z \to \infty$

$$\phi(x,\infty) = - \phi_o \, e^{-x^2/L_x^2} \tag{3.2}$$

and

$$\phi(x,o) = - \phi_o \, (1 - A) \, e^{-x^2/L_x^2} \tag{3.3}$$

For large z (usually $z/L_z \gtrsim 3$), the potential remains nearly unchanged along the z direction, and appears as a parallel equipotential structure.

The potential drop along the magnetic field lines (assuming in the z direction) can be obtained from equations (3.2) and (3.3)

$$\Delta\phi(x) = \phi(x,o) - \phi\,(x,\infty) \tag{3.4}$$

$$= A \, \phi_o \, e^{-x^2/L_x^2}$$

The curve $\Delta\phi(x)$ is shown at the bottom of Figure 3.3.

The two-dimensional potential function (3.1) is of a Gaussian shape in the x direction. It is notable that the Gaussian distribution of the electric potential in the perpendicular direction is the zero-order approximation of the solution to the Poisson equation in one-dimensional case for the inverted-V, under

the assumption that the electron number density profile at the source is assumed to be Gaussian (Kan et al., 1979).

3.2. S-shape

The potential function for S-shape structure is assumed to be

$$\phi(x,z) = \begin{cases} \phi_o \left[e^{-x^2/L_x^2} + \left(e^{-x^2/(\gamma \cdot L_x^2)} - e^{-x^2/L_x^2} \right) \cdot \left(1 - e^{-z^2/L_z^2} \right) \right], & x \geq 0 \\ \phi_o & x < 0 \end{cases} \tag{3.5}$$

where ϕ_o is the magnitude of the electric potential, L_x and L_z are scale lengths in the x and z direction; γ is a characteristic parameter, which expresses the ratio of the transverse electric potential scale at

$z \to \infty$ altitude and that at $z = 0$ altitude, $\gamma \leq 1$.

From equation (3.5)

$$\phi(x,\infty) = \phi_o e^{-x^2/(\gamma \cdot L_x)^2} \tag{3.6}$$

$$\phi(x,o) = \phi_o e^{-x^2/L_x^2} \tag{3.7}$$

and the potential drop along the magnetic field

$$\Delta\phi(x) = \phi_o \left(e^{-x^2/L_x^2} - e^{-x^2/(\gamma \cdot L_x)^2} \right) \tag{3.8}$$

Figure 3.4 shows the equipotential lines for an S-shaped potential field with $L_x^* = 1.5$, $L_z^* = 20.0$, and $\gamma = 0.25$. The curve of the potential drop $\Delta\phi(x)$ is drawn at the bottom of the figure. So far, we do not have much observational information about the topology of the S-shape potential. The equipotential shape shown in Figure 3.4 is similar to that given by Mozer et al. (1980).

The curve of $\Delta\phi(x)$ given by equation (3.8) is an asymmetrically inverted V-shape, while equation (3.4) for V-shaped cases gives a symmetrically inverted V.

4. Trajectories

The study of the motions of the individual charged particles in the V-shaped and S-shaped potential is useful and important for our understanding of the collective dynamics of the plasma in those regions. But due to the complexities of the particle orbits, which appear different with different characteristic parameters or different initial conditions in the potential models, it is very difficult to solve the equations of motion analytically, especially in nonabiabatic cases. However, we can use some approximations to analyze the particle behaviors. These will be discussed in Section 5. A comprehensive numerical study of the trajectories of nonadiabatic particles ($L_x \sim \rho_i$, $L_x < \rho_i$) will be presented in this section by following.

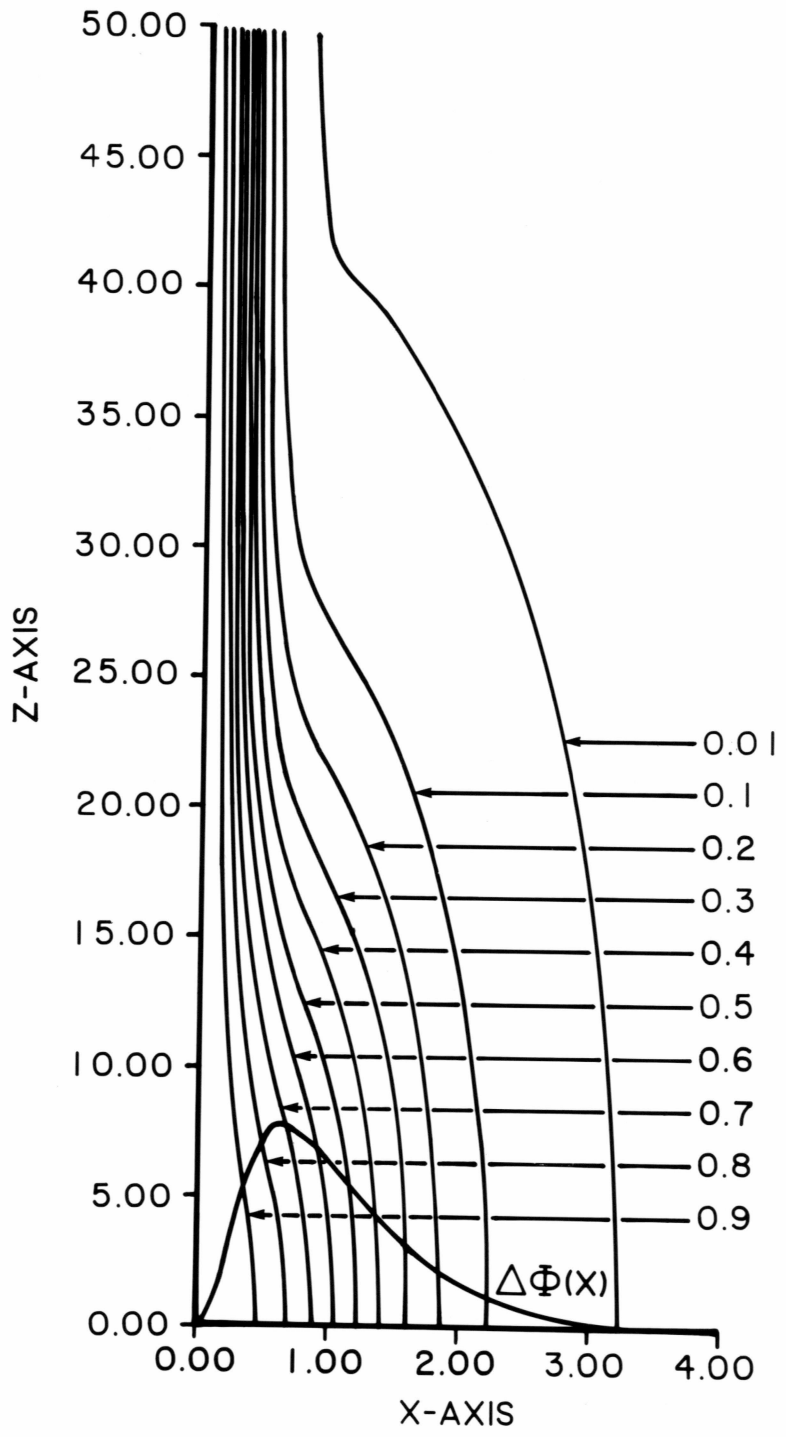

Figure 3.4 Illustration of a S-shaped equipotential structure (L_x=1.5, L_z=20.0, γ=0.25).

It should be mentioned that a numerical study of particle trajectory in plasma sheet has been done previously by Wagner et al. (1979).

4.1. Basic Equations

For convenience, we assume that the magnetic field is uniform, and it orients the z direction.

The equation of motion for a charged particle of mass m and charge q in an electromagnetic field is given by the Lorentz equation

$$m\ddot{\vec{r}} = q[\vec{E}(\vec{r},t) + \dot{\vec{r}} \times \vec{B}(\vec{r},t)] \tag{4.1}$$

To simplify our computation, it is advantageous to write the equations of motion in dimensionless form. All the lengths and times are scaled, respectively, to a scaling gyroradius $\rho_o = mv_o/qB_o$, and to a scaling gyroperiod $\tau_o = m/qB_o$.

The dimensionless equations of (4.1) in two-dimensional electric field $\vec{E}(x,z)$ can be written

$$\frac{d\dot{x}^*}{dt^*} = E_x^* + \dot{y}^*$$

$$\frac{d\dot{y}^*}{dt^*} = -\dot{x}^* \tag{4.2}$$

$$\frac{d\dot{z}^*}{dt^*} = E_z^*$$

where $\vec{r}^{*} = \vec{r}/\rho_o$, $t^{*} = t/\tau_o$, $\dot{\vec{r}}^{*} = \dot{\vec{r}}/v_o$, $E^{*} = E/v_o B_o$ and $B^{*} = B/B_o = 1$.

E_x^{*} and E_y^{*} are easy to deduce from equation (3.4) and equation (3.5) for V-shaped and S-shaped potentials, respectively.

In the following calculation, ρ_o is taken from the gyroradius of the test particle (m,q) with kinetic energy 0.5 keV in magnetic field B_o. For example, choose $B_o = 0.06$ G, for proton, $\rho_o = 0.54$ km; for O^{+}, $\rho_o = 2.2$ km.

The charged particles are assumed to originate from z = 0 plane with a low energy (1 eV). It is found that the initial pitch angles and phase angles are not important when the initial energy of the particle is very small compared with the final kinetic energy gain. The initial position x_o^{*} of the test particles is the deciding factor for low-energy ions. So we usually let the initial pitch angle be 45^{o}, initial phase angle 0^{o}. With this setting, trajectories originating from different initial position x_o^{*} are investigated.

It should be noted, the figures of the orbits shown in this section have different scales in all the x^{*}, y^{*} and z^{*} directions, such that the whole trajectory in each direction can be seen clearly in the plot.

4.2. Trajectories in V-shaped Potential Models

Case (A): ϕ_o = 8 KV, L_x^* = 1.5, A = 0

This is a special case (A = 0) of V-shaped for the parallel equipotential configuration. The initial kinetic energy of the test particle is assumed to be 1 eV. The figures 4.1 (a), (b) and (c) show the projections on the $x^* - y^*$ plane of the orbits of the test particles with the initial position x_o^* = 0.8, 3.2 and 3.6, respectively.

Oscillations in the x^*-direction are the common feature of the motion in the parallel equipotential configuration. The maximum perpendicular kinetic energy gain is determined by the amplitude of the oscillation. In most cases the pitch angles are very close to 90^o.

For the x_o^* = 0.8 case, the particle moves across the x^* = 0 plane, and attains the maximum kinetic energy at the position x^* = 0. When the particle reaches the region of $x^* < 0$, it suffers an opposite force in the x^* direction, because of the reverse of electric field. The period of the oscillation T^* = 2.1. The maximum kinetic energy gain is 2 keV.

For the x_o^* = 3.2, the particle can also be accelerated across the magnetic field from the origin, where the electric field is much weaker than that in x_o^* = 0.8. The mechanism of this acceleration will be discussed in Section 5. The particle oscillates across the x^* = 0 plane, and the period T^* = 9.3. The maximum kinetic energy gain is 7.92 keV.

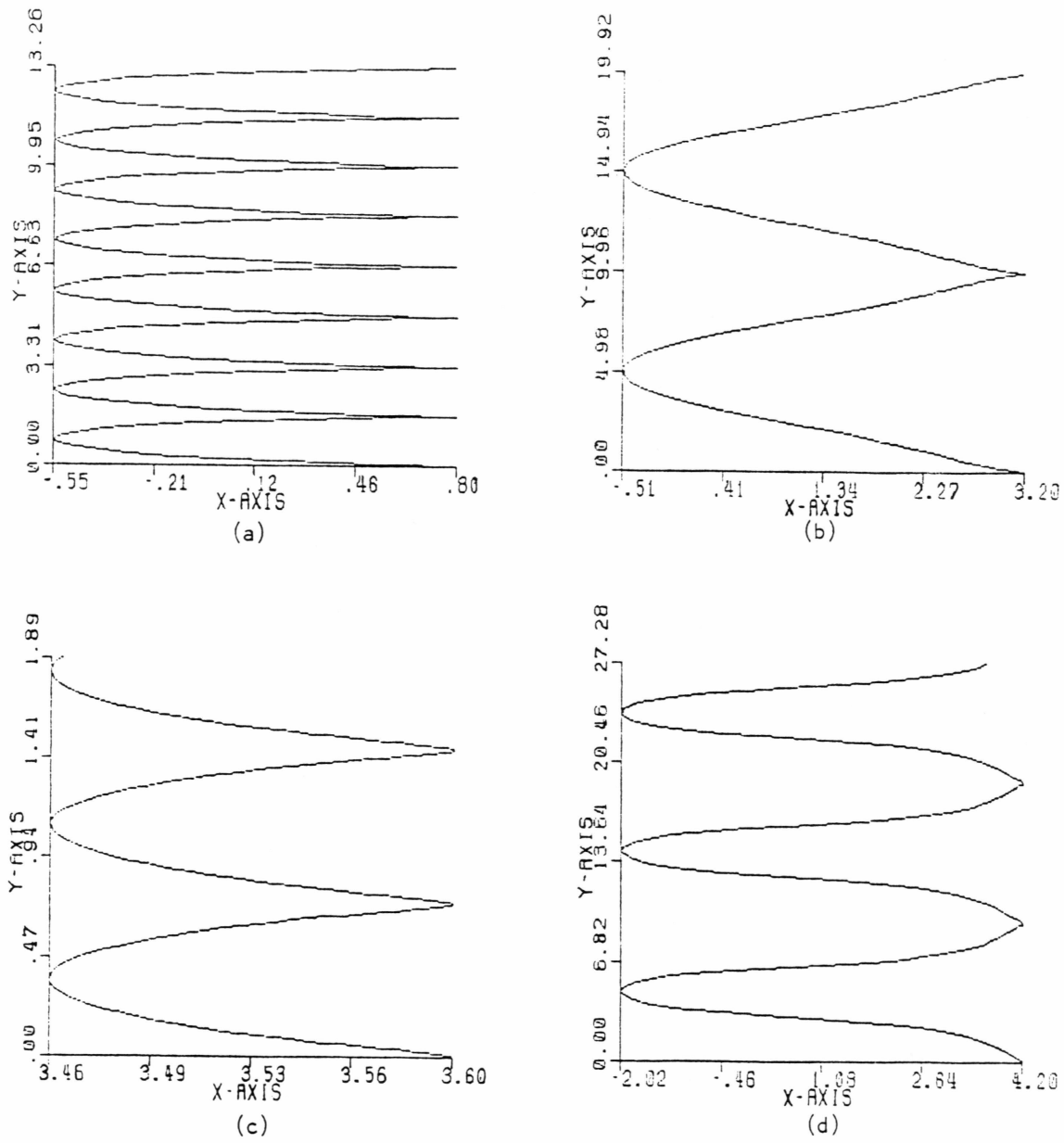

Figure 4.1 Projections of a Case A particle trajectory in a V-shaped potential model.

For the $x_o^* = 3.6$ case, Figure 4.1 (c) shows that the amplitude of the oscillation becomes very small, and the corresponding maximum kinetic energy gain for the particle sharply reduces to 18 eV. The period of motion for this case is, $T^* = 6.9$.

Let us assume that the lengths are scaled to the gyroradius of the proton with kinetic energy 0.5 keV. Figure 4.1 (d) shows that trajectory of a O^+ ion in the same potential. The initial position of the O^+ ion is, $X_o^* = 4.2$. The O^+ ion can be energized by the perpendicular electric field, and attains its maximum kinetic energy gain, $E_k = 8.0$ keV at $X^* = 0$. The period of the oscillation is, $T^* = 196$. We can find that the O^+ ions have a larger acceleration range than H^+.

Case (B): $\phi_o = 8$ KV, $L_x^* = 1.5$, $L_z^* = 20$, $A = 1$

This is another special case for a pure V-shaped potential ($A = 1$). The configuration of this potential has been shown previously in Figure 3.3.

Figure 4.2 shows the particle trajectory with the initial position $x_o^* = 1.5$. The particle moves up slowly, then accelerates obviously both in perpendicular and parallel direction. In this energization process, the parallel acceleration is larger than the perpendicular acceleration. Finally, the particle oscillates in the x^* direction with a small amplitude $\Delta x^* \sim 0.05$, drifts in the y^* direction, and moves up in the z^* direction with a uniform velocity. The final values are, the pitch angle $\alpha \sim 20^o$, $V_x^* =$

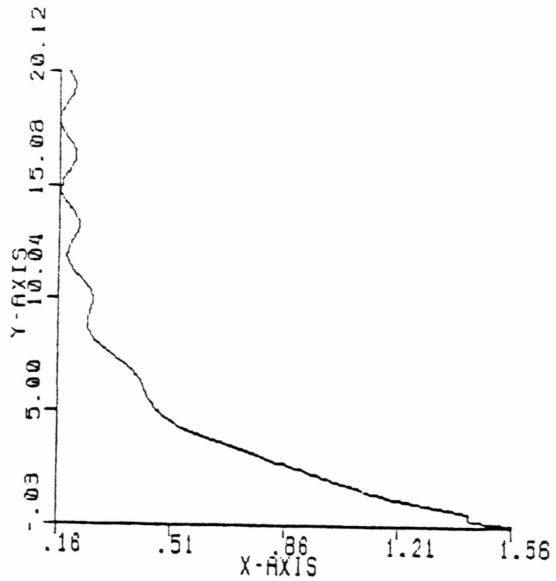

PARTICLE TRAJECTORY PLOT
L_x=1.5, L_z=20.0, Φ_0=8.0
INITIAL VALUES:
X=1.5000, Y=0.0000, Z=0.0000
Vx=0.0000, Vy=0.0316, Vz=0.0316
ENERGY=0.0010
PITCH=45.0°, PHASE=0.0°
FINAL VALUES:
X=0.1977, Y=20.1246, Z=50.3287
Vx=-0.0646, Vy=1.3339, Vz=3.7302
ENERGY=7.8493
PITCH=19.6°, PHASE=2.7°

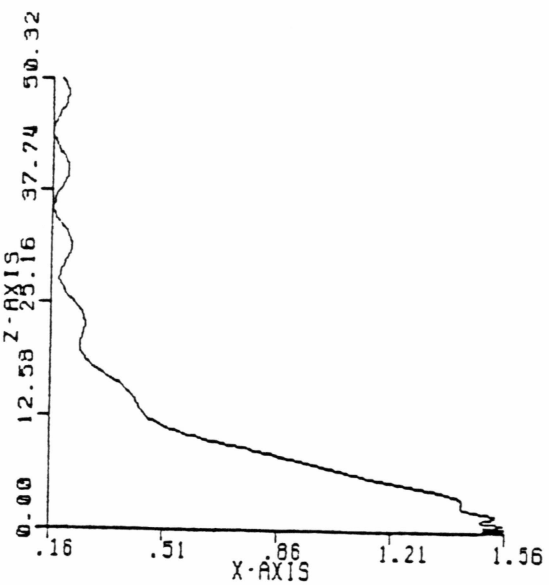

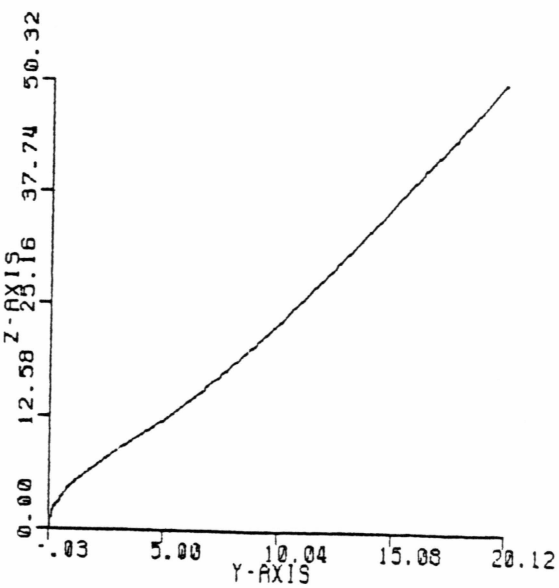

Figure 4.2 Projections of a Case B particle trajectory in a V-shaped potential model ($x_o^* = 1.5$).

-0.06, $V_y^* = 1.33$, $V_z^* = 3.73$, and the kinetic energy $E_K \sim 7.85$ keV.

Figure 4.3 shows the trajectory with the initial position $x^* = 3.2$. The main feature of this energization process is a sharp increase of acceleration in the x^* direction when the test charged particle moves and is accelerated up slowly in the z^* direction to a certain altitude ($z^* \sim 20$). The perpendicular acceleration in this process is similar to that shown in Figure 4.1 (a). The difference is that the particle in the V-shaped potential also gains energy in the parallel direction. The final pitch angle varies between 45° - 70°, while the final kinetic energy varies between 2.7 - 8.0 keV, during the oscillation of the up-moving particle.

Figures 4.4 (a) and (b) show the relations between the final kinetic energy of the test-charged particle and the initial position x_o^*, and between the final pitch-angle value and the initial position x_o^* at a high altitude, where the electric field in the z^* direction nearly vanishes. Each bar in the figures shows the variation range of the values of the kinetic energy and the pitch angle of the test particle when it is oscillating in the x^* direction. The pitch-angle distribution ranges from 0° to 80°, while the kinetic energies from several eV to $e\phi_o$ (8 keV).

From Figure 4.4 (a), we can see a sharp "cut off," which happens at $x_o^* \sim 3.4$. When $x_o^* > 3.4$, there is no significant acceleration in all directions. This phenomenon has the same physical nature as the case shown in Figure 4.1 (c).

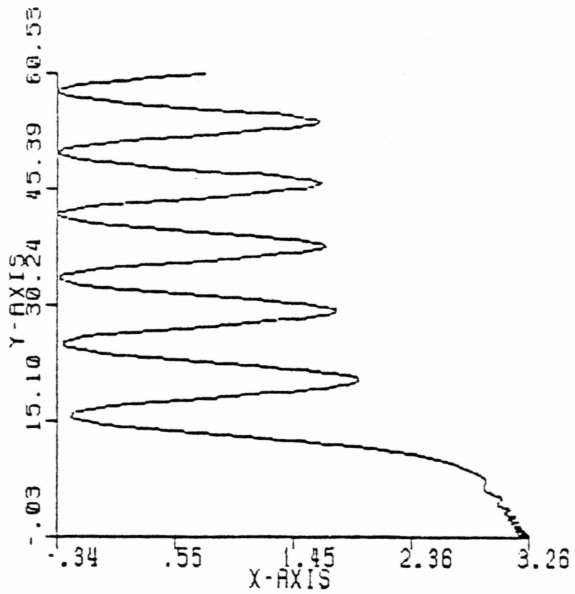

PARTICLE TRAJECTORY PLOT
L_x=1.5, L_z=20.0, Φ_o=8.0
INITIAL VALUES:
X=3.2000, Y=0.0000, Z=0.0000
Vx=0.0000, Vy=0.0316, Vz=0.0316
ENERGY=0.0010
PITCH=45.0°, PHASE=0.0°
FINAL VALUES:
X=0.7863, Y=60.5307, Z=50.1381
Vx=1.9739, Vy=2.4453, Vz=1.5030
ENERGY=6.0674
PITCH=64.4°, PHASE=-38.9°

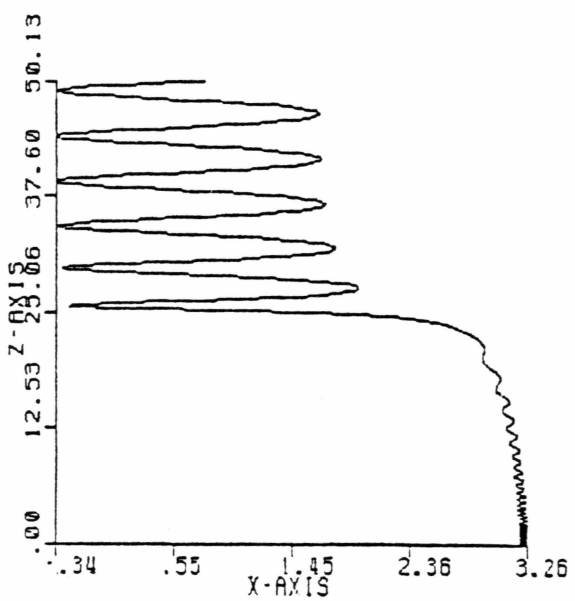

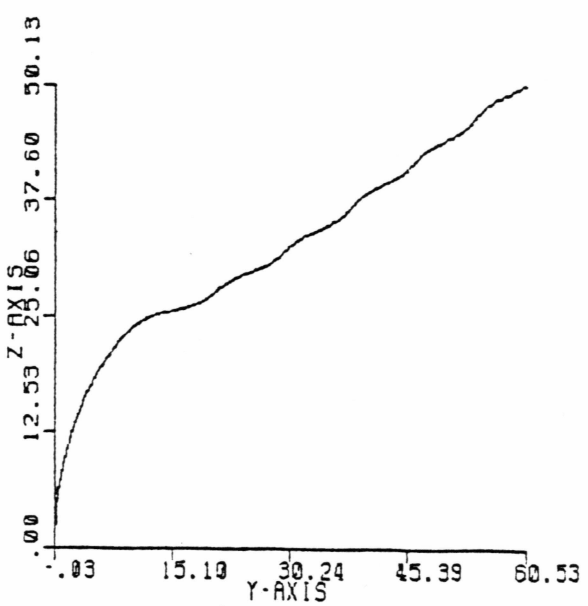

Figure 4.3 Projections of a Case B particle trajectory in a V-shaped potential model ($x_o^* = 3.2$).

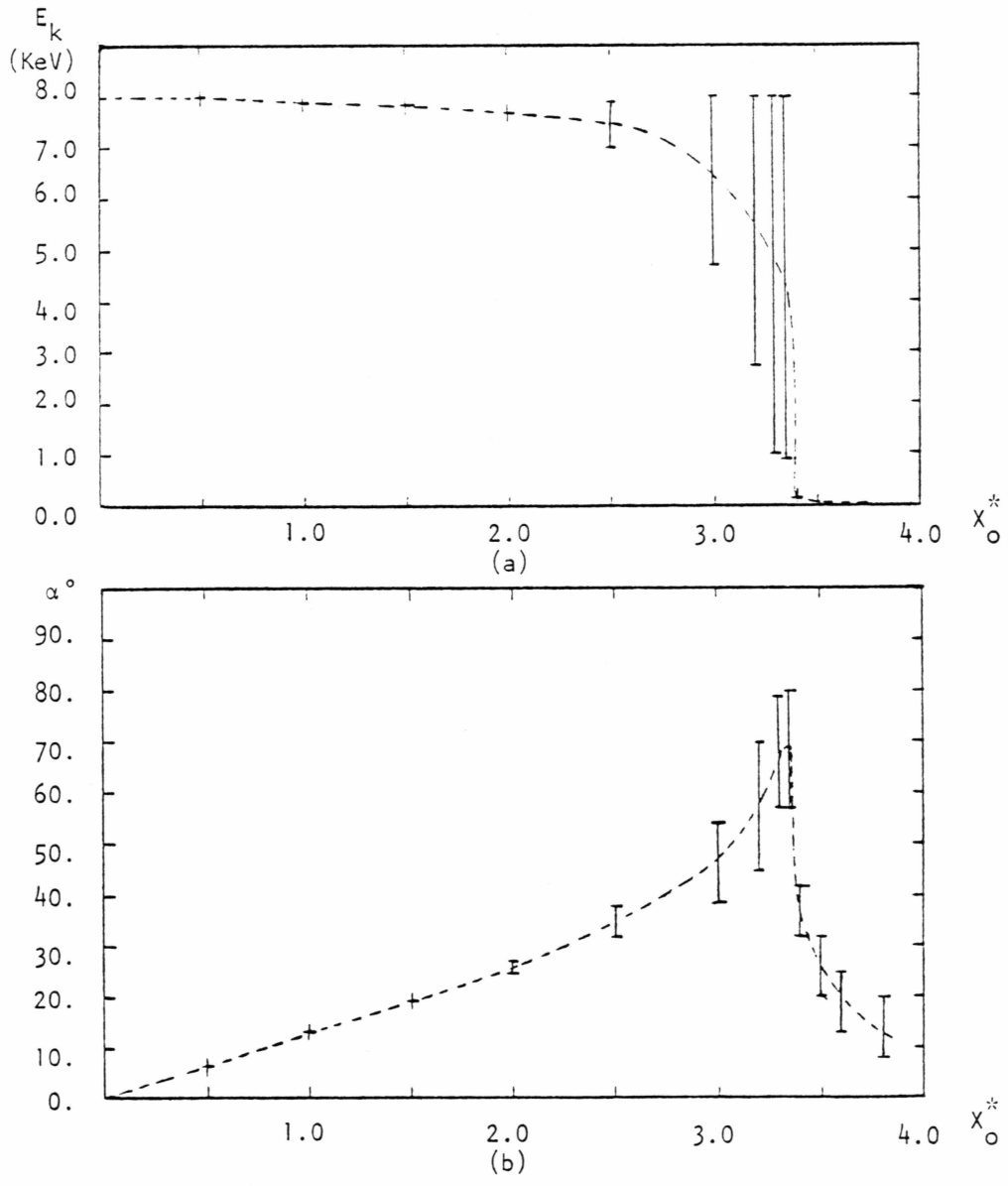

Figure 4.4 Results of the trajectory study of Case B in a V-shaped potential model

(a) relation between the final kinetic energy E_K and the initial position x_o^*.

(b) relation between the final pitch-angle value α and the initial position x_o^*.

If we assume a uniform number density distribution at the origin of the ions, namely at the $z^* = 0$ plane, the final kinetic energy distribution of the energized particle peaks at the values close to $e\phi_o$ (8 keV). Because the particles have the tendency towards the central part of the V-shaped potential, as shown in Figure 4.2, an intense flux of energetic particles will be formed in a region of $|x^*| \lesssim 0.5$ at a high altitude. In this region most particles have pitch angles smaller than 30^o.

Case (C): $\phi_o = 8$ KV, $L_x^* = 1.5$, $L_z^* = 20.0$, $A = 0.4$

Figure 4.5 shows the trajectory of a test-charged particle originating at $x_o^* = 3.0$. The initial acceleration in the x^* direction plays an important role in this process. As a result of the acceleration, the particle finally oscillates in the x^* direction with an amplitude $\Delta x^* = 1.73$. The final pitch angle varies in the range $38^o - 61^o$, while the kinetic energy in the range 3.0 - 7.9 keV. The particle attains its maximum pitch angle value and maximum kinetic energy when it moves across the $x^* = 0$ plane.

The results of this study are shown in Figure 4.6 (a) and (b). The kinetic energy gain for the energized charged particles peaks at 0.5 - 0.6 $e\phi_o$ (4 - 5 keV). A sharp "cut off" can be seen at $x_o^* \sim 3.4$ in the Figure 4.6 (a). From Figure 4.6 (b), it is obvious that the particles have larger pitch angles compared to that in A = 1 case. Most particles have pitch angles in the range of $15^o - 50^o$.

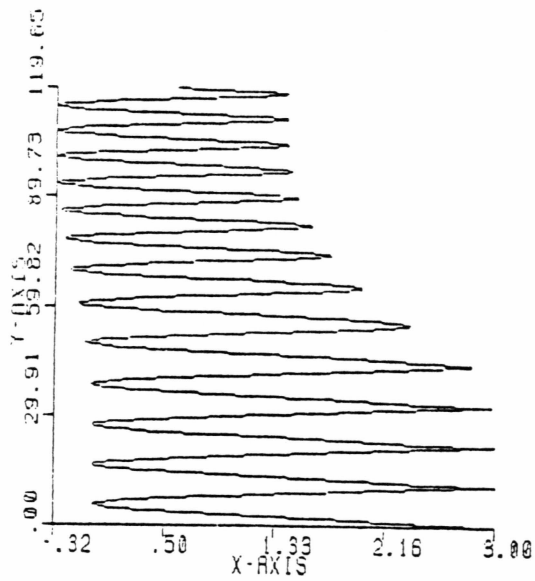

PARTICLE TRAJECTORY PLOT
L_x=1.5, L_z=20.0, ϕ_o=8.0, A=0.4
INITIAL VALUES:
X=3.0000, Y=0.0000, Z=0.0000
Vx=0.0000, Vy=0.0316, Vz=0.0316
ENERGY=0.0010
PITCH=45.0°, PHASE=0.0°
FINAL VALUES:
X=0.5820, Y=119.6527, Z=50.0344
Vx=-1.9515, Vy=2.4496, Vz=1.9418
PITCH=58.2°, PHASE=38.5°
ENERGY=6.7898

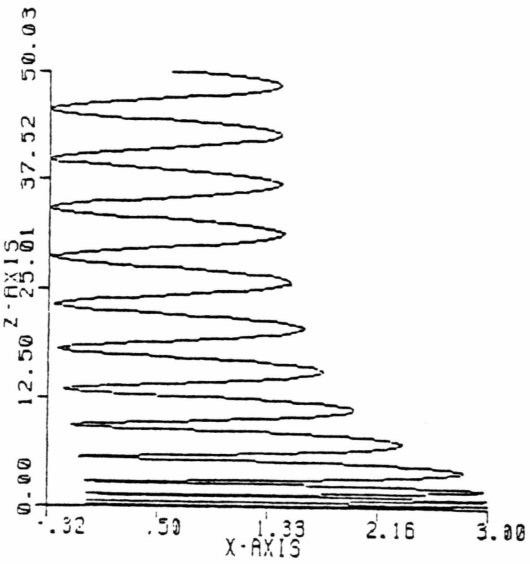

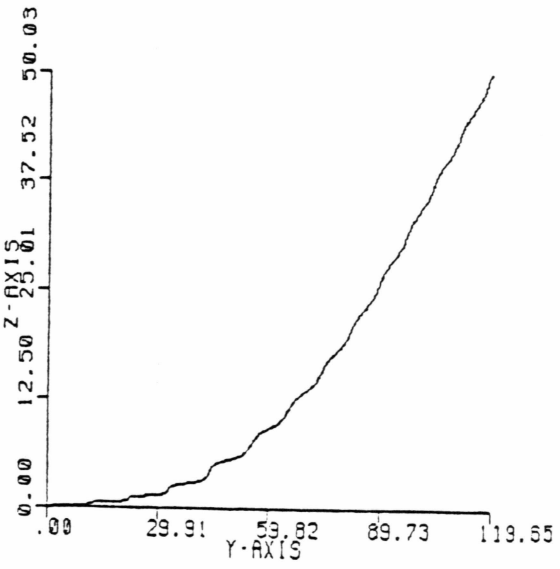

Figure 4.5 Projections of a Case C particle tajectory in a V-shaped potential model.

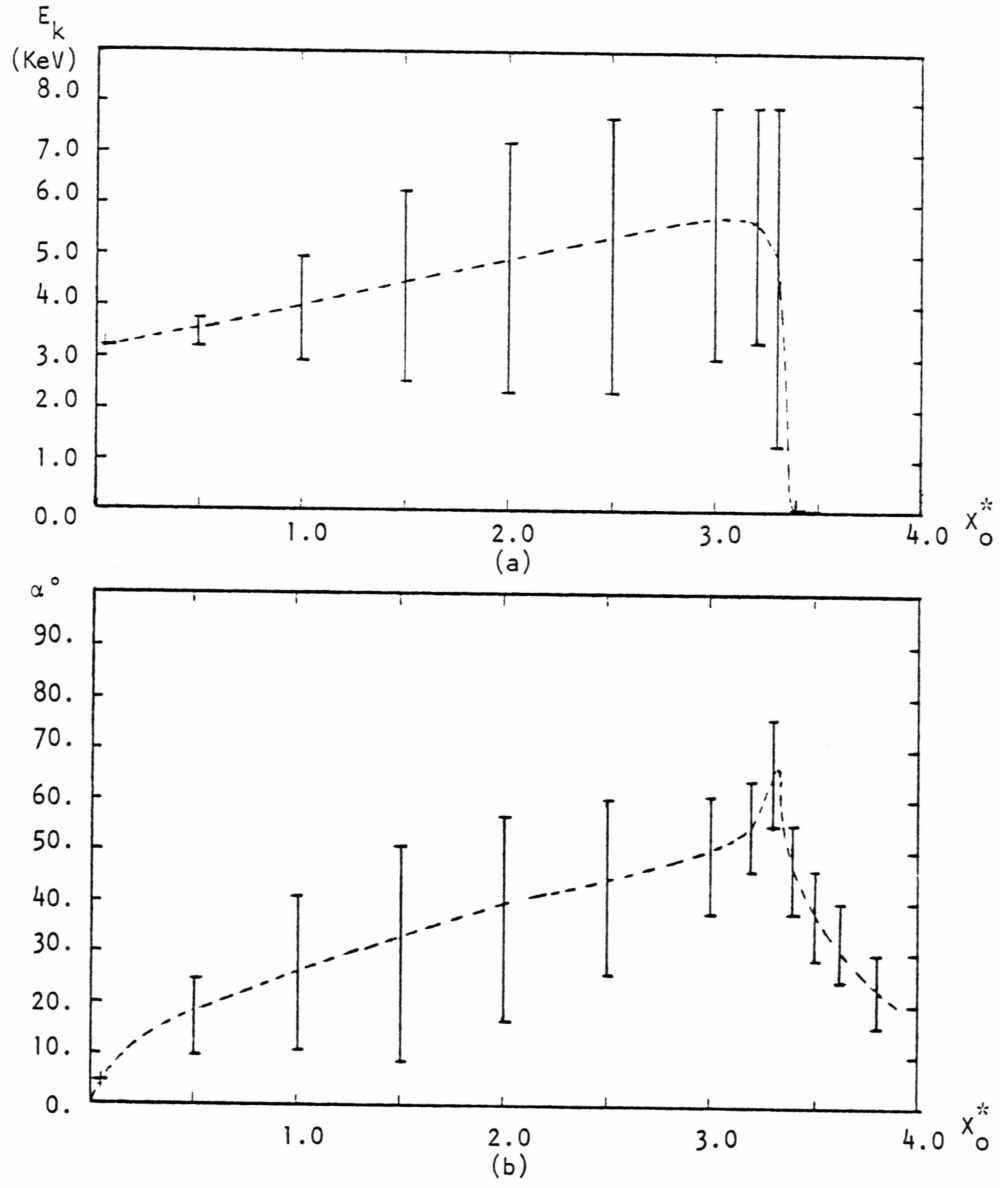

Figure 4.6 Results of the trajectory study of Case C in a V-shaped potential model

(a) relation between the final kinetic energy E_K and the initial position x_o^*.

(b) relation between the final pitch-angle value α and the initial position x_o^*.

The trajectory study also shows that the perpendicular acceleration will increase when the parameter A decreases. This parameter modulates the shape of the equipotential lines of the potential field. When A increases, the field model given by equation (3.1) approaches the limit of the pure V-shaped configuration (A = 1); while A decreases, it approaches the limit of the parallel equipotential configuration (A = 0), in which case the perpendicular acceleration dominates and the particles can be expected to attain larger pitch angles.

Case (D): ϕ_o = 8 KV, L_x^* = 3.0, L_z^* = 20.0, A = 1

Figure 4.7 shows an example of the trajectories in this potential field. The initial position is x_o^* = 4.0. The final kinetic energy gain is about 5.64 keV, and the velocity components are V_x^* = 0.053, V_y^* = 2.26, and V_z^* = 2.49. It is interesting to note that the final perpendicular energy gain in y^* direction is much larger than that in the x^* direction. The final pitch angle is about 42.2°.

One characteristic of these orbits is the fact that the amplitudes of final oscillations in x_o^* direction are quite small. So the variation of the pitch-angle value and also the kinetic energy value of the upward-moving particles is small at the high altitude. Thus it is simple to estimate the latitudinal distributions of the pitch angle α, the kinetic energy E_K, and the average number density rate n/n_o at the high altitude. Here, a

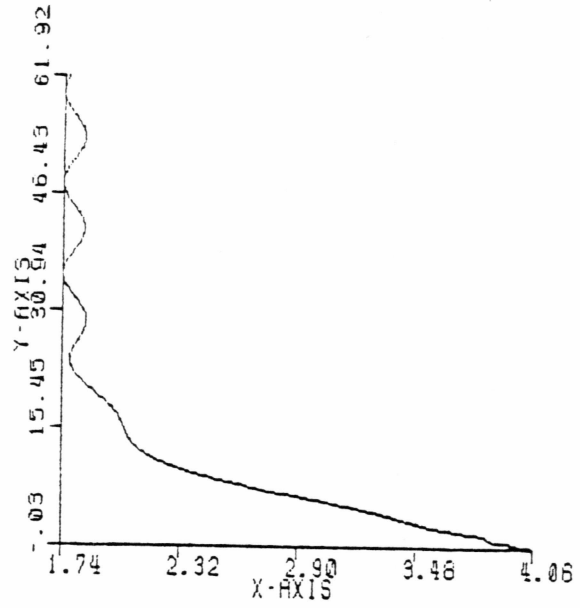

PARTICLE TRAJECTORY PLOT
L_x=3.0, L_z=20.0, Φ_c=8.0
INITIAL VALUES:
X=4.0000, Y=0.0000, Z=0.0000
Vx=0.0000, Vy=0.0316, Vz=0.0316
ENERGY=0.0010
PITCH=45.0°, PHASE=0.0°
FINAL VALUES:
X=1.7730, Y=61.9293, Z=80.0667
Vx=0.0526, Vy=2.2586, Vz=2.4862
Energy=5.6425
PITCH=42.2°, PHASE=-1.3°

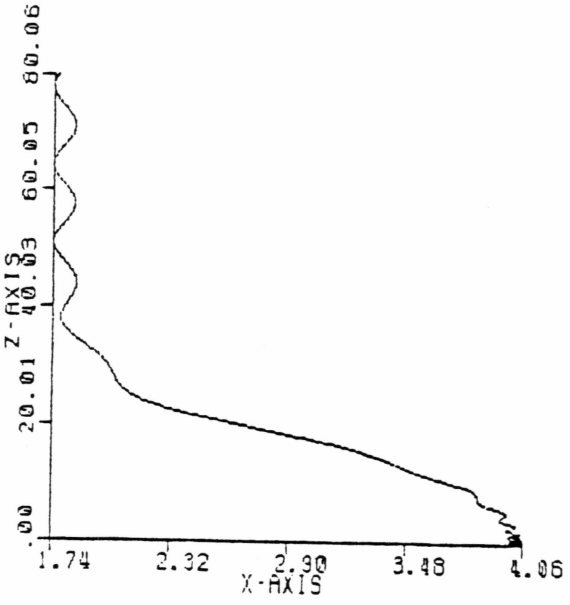

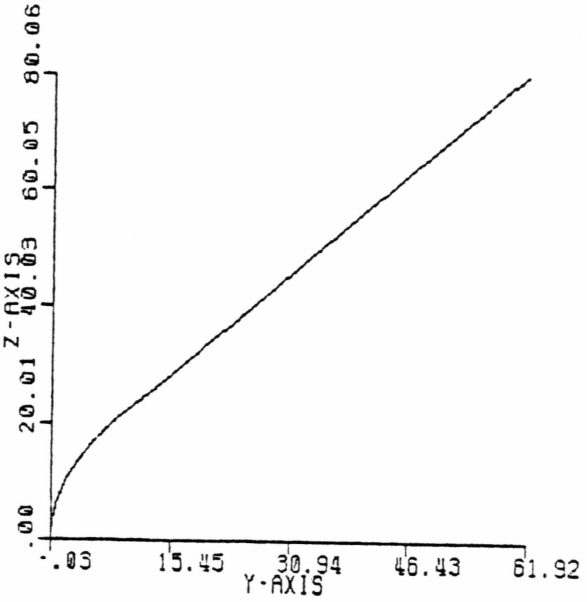

Figure 4.7 Projections of a Case D particle trajectory in a V-shaped potential model.

uniform distribution of the number density n_o of the origin at $z^* = 0$ is assumed. The curves are shown in Figure 4.8. At the bottom of the figure, the dots at the x_o^* axis show the original positions of the test particles. The arrows direct towards the final positions of the particles. Within the acceleration region, i.e., $|x_o^*| \lesssim 2.5$, the latitudinal distribution of the number density at the high altitude will attain its maximum value in the region $|x^*| \lesssim 1.0$, in which the kinetic energy ranges from 7.5 - 8 keV, and the pitch angle ranges from 0 - 20°.

4.3 Evaluation of the Action Integral

The action integral for an oscillatory system is defined

$$J = \oint p dq \qquad (4.3)$$

where the integral is calculated around a loop in a (p,q) phase space (Lichtenberg, 1969). Swift (1979) studied the ion behaviours in two-dimensional laminar electrostatic shocks with thicknesses close to ρ_i, under the assumption of the adiabatic invariance of the action integral.

The following are the results of calculating the action integrals for Case (B) of Section 4.2, i.e., the V-shaped potential given by ϕ_o = 8 KV, L_x^* = 1.5, L_z^* = 20, and A = 1. Two trajectories of the test particle are shown in Figure 4.2 and Figure 4.3. Let

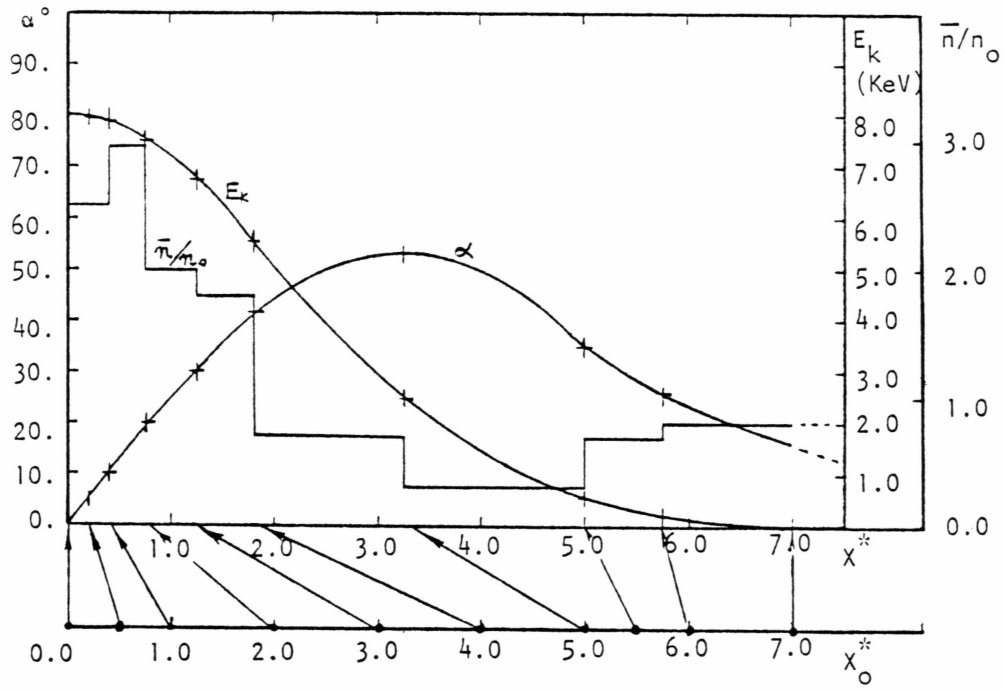

Figure 4.8 Latitudinal distribution of final pitch angle α, kinetic energy E_K, and relative number density n/n_o for Case D in a V-shaped potential model.

$$K^* = \oint v_x^* \, d x^* \tag{4.4}$$

We assume that the initial value of the action integral is K_1^*, and the final value of the action integral is K_2^*.

(i) For trajectory shown in Figure 4.2, i.e., $x_o^* = 1.5$

$$K_1^* = 2.4 \cdot 10^{-3}$$

$$K_2^* = 4.8 \cdot 10^{-3} \tag{4.5}$$

(ii) For trajectory shown in Figure 4.3, i.e., $x_o^* = 3.2$

$$K_1^* = 3.0 \cdot 10^{-3}$$

$$K_2^* = 5.33 \tag{4.6}$$

From these results, we can see that for a small scale electric potential, i.e., $L_x \lesssim 0.7\ \rho_i$, the action integral will not be invariant, especially for those particles which could obtain large energy gain in oscillation.

4.4 Trajectories in S-shaped Potential Models

The main difference of the acceleration in the S-shaped potential from that in the V-shaped potential is that there is no reverse electric field appearing in the process.

Case (A): ϕ_o = 8 KV, L_x^* = 1.5, L_z^* = 20.0, γ = 0.25

An example of the trajectries in this potential is shown in Figure 4.9. The initial position is x_o^* = 0.5. The perpendicular acceleration dominates during the initial periods. Finally, the particle oscillates in the x^* direction with an amplitude ~ 3.56 . The pitch angle varies in the range 6^o - 60^o, and the kinetic energy in the range 1.9 - 7.2 keV.

The kinetic energy gain decreases gradually when the original position x_o^* increases. When $x_o^* > 3.4$, the kinetic energy gain of the particle is negligible. The maximum pitch-angle values for most the energized particles range about 40^o - 65^o.

4.5 Comparison Between O^+ and H^+ Trajectories

The different dynamic behaviors of H^+ and O^+ in the V-shaped potential are investigated by the trajectory study. The following are the results of the study.

(a) In the pure V-shaped potential, ϕ_o = 8 keV, $L_x^* \lesssim 2$ (length scaling in the H^+ gyroradius), L_z^* = 20.0, A = 1, there is no large difference in the O^+ and H^+ energy distribution and pitch-angle distribution, as both the O^+ and H^+ ions in their acceleration regions can attain the maximum kinetic energy gains which are close to $e\phi_o$(8 keV) when moving cross or close to the x^* = 0 plane. Obviously O^+ has a larger acceleration region and a larger amplitude of the oscillation.

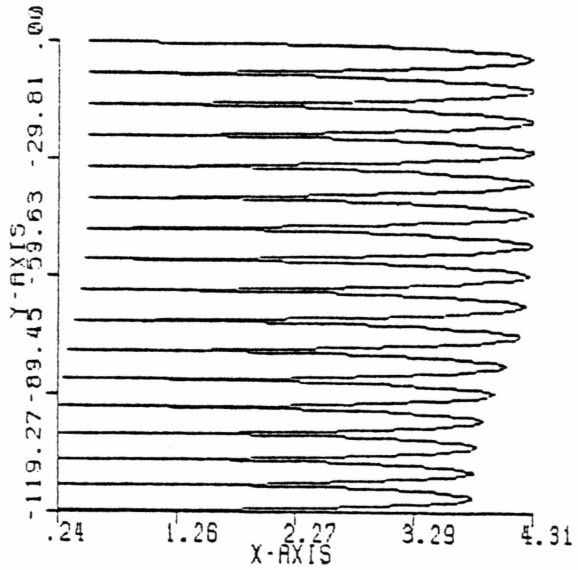

PARTICLE TRAJECTORY PLOT
L_x=1.5, L_z=20.0, Φ_o=8.0, γ=0.25
INITIAL VALUES:
X=0.5000, Y=0.0000, Z=0.0000
Vx=0.0000, Vy=0.0316, Vz=0.0316
ENERGY=0.0010
PITCH=45.0°, PHASE=0.0°
FINAL VALUES:
X=2.1501, Y=-119.2735, Z=50.0679
Vx=2.8338, Xy=-1.6184, Vz=1.9146
ENERGY=7.1578
PITCH=59.5°, PHASE=-119.7°

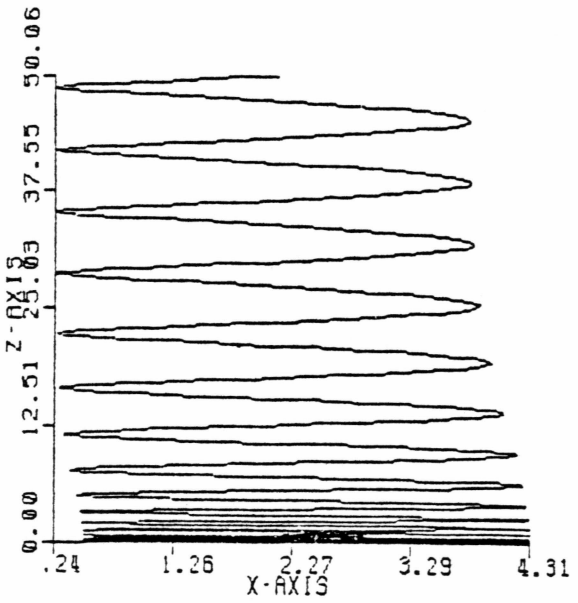

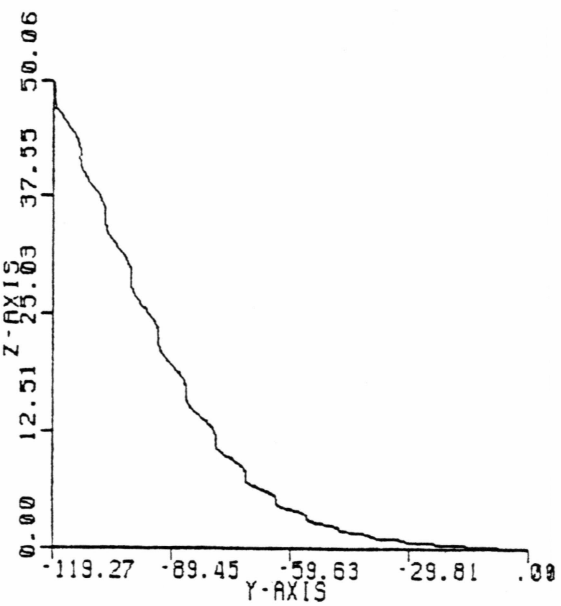

Figure 4.9 Projections of a Case A particle trajectory in a S-shaped potential model.

For $L_x^* \sim 3$, the H^+ trajectory has been studied previously in Section 4.2.4., shown in Figure 4.7. In these cases, the trajectories of O^+ still have the patterns of crossing the $x^* = 0$ plane motion. O^+ ions obviously have larger kinetic energy gains than H^+ ions. But as the energy gain is both in perpendicular and parallel direction, here is no evidence that the O^+ pitch-angle distribution peaks at a larger value than H^+.

(b) Figure 4.10 shows a comparison of the trajectories of the O^+ and H^+ in a V-shaped potential, $\phi_o = 8$ KV, $L_x^* = 5.0$, $L_z^* = 20.0$, $A = 0.4$. For O^+(1 eV) originated at $x_o^* = 6.0$, the final kinetic energy ranges from 4.2 - 6.8 keV, and the pitch angle ranges from 43^o - 55^o. For O^+ with initial position, $x_o^* = 1.0$, the final kinetic energy ranges from 3.1 - 4.6 keV, and the pitch angle ranges from 11^o - 34^o. This trajectory is not shown in the figure.

For H^+, $x_o^* = 6.0$, the final kinetic energy is about 2.7 keV, and the pitch angle is $\sim 49^o$; $x_o^* = 1.0$, the final energy $E_K \sim 3.2$ keV and the pitch angle $\alpha \sim 12^o$. In these cases, the drift motion in the y^* direction dominates in the final perpendicular kinetic energy gain.

On the average, the O^+ can attain larger kinetic energy and larger pitch angle than H^+. This will be more distinct in the region around the $x^* = 0$ plane, for example $|x^*| < 1$, over where O^+ ions from a wide range can attain their maximum kinetic energy and maximum pitch angles. For O^+ ions originating in the region $1.0 \lesssim |x_o^*| < 11.0$, the pitch angle ranges from 30^o - 85^o, and the

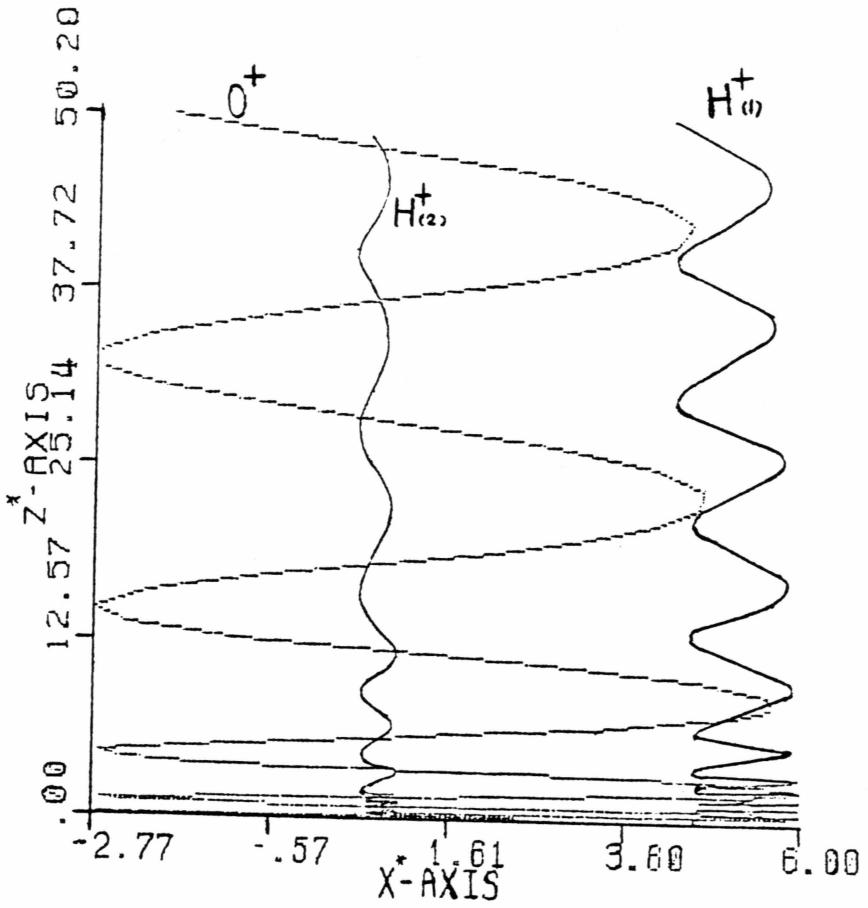

Figure 4.10 A comparison of 0^+ and H^+ trajectories in a V-shaped potential, ϕ_o = 8 kV, L_x^* = 5.0, L_z^* = 20.0, A = 0.4.

kinetic energy ranges from 4.2 - 7.5 keV in the region $|x^*| < 1$. As for H^+, only those ions from a small region $|x_o^*| \lesssim 1.2$, can oscillate in the observing region. The possible pitch angle value is smaller than 13^o, and the final kinetic energy is around 3.3 keV.

(c) Another case we investigated is the ion behavior in a larger transverse scale electric field, in which the H^+ ion orbits exhibit adiabatic behavior. The H^+ ions move up with small pitch angles. The kinetic energy gain can be estimated from $\Delta\phi(x)$ of equation (3.4). And O^+ might still attain pitch angles larger than 10^o, which is considered a criterion from beam to conic phenomenon by many upflowing ion observers.

In a pure V-shaped potential field, $\phi_o = 8$ KV, $L_x^* = 20.0$, $L_z^* = 100.0$, $A = 0$, the final values for H^+ originated at $x_o^* = 10.0$ are, $E_K \sim 6.3$ keV, $\alpha \sim 4.4^o$; for O^+ ($x_o^* = 10.0$), $E_K \sim 7.2$, and $\alpha \sim 14^o$.

In a V-shaped potential field, $\phi_o = 8$ KV, $L_x^* = 40.0.$, $L_z^* = 100.0$, $A = 0.4$, the final values for H^+ ($x_o^* = 10.0$) are $E_K \sim 2.5$ keV, $\alpha \sim 3.6^o$; for O^+ ($x_o^* = 10.0$), $E_K \sim$ 2.6 - 3.2 keV, $\alpha \sim 7.1^o - 23^o$.

5. Theoretical Analysis of Non-adiabatic Particle Dynamics

The purpose of this section is to understand the numerical results (in Section 4) from a theoretical point of view. Cole (1976) has developed a criterion for perpendicular ion acceleration

in a one-dimensional electric field. We show that the ion dynamics in the two-dimensional V and S potential structures can be understood by a generalization of Cole's (1976) work.

(1) Cole (1976) has examined the motion of charged particles, in the case of a homogeneous magnetic field $\vec{B}$ together with an orthogonal electric field $\vec{E}$. The equation of motion was solved for the case that the electric field $\vec{E}$ has a constant gradient ∇E parallel to $\vec{E}$. The solution gives a critical value for the charged particle motion: if $\nabla E < \frac{qB^2}{m}$, the particle drifts at a right angle to $\vec{E}$ and $\vec{B}$ with a modified gyrofrequency $\Omega = (\omega^2 - \frac{q\nabla E}{m})^{1/2}$, $\omega = \frac{qB}{m}$; if $\nabla E > \frac{qB^2}{m}$, the particle not only drifts in the direction of $\vec{E} \times \vec{B}$ but are also accelerated in the direction of $\vec{E}$. This relation is mass dependent. For B = 0.06 G, the critical value $\nabla E = 3.42$ mv/m^2, for H^+; and $\nabla E = 0.21$ mv/m^2, for O^+. This mechanism operates more efficiently on O^+ than H^+, so acceleration by perpendicular electric fields may be more important for oxygen than for hydrogen.

Figure 5.1 illustrates the movement of a positively charged particle in crossed $\vec{E}$ and $\vec{B}$ fields, in which constant ∇E exists parallel to $\vec{E}$. The two different patterns of orbits are separated by the critical value

$$\nabla E = \frac{qB^2}{m} = \frac{m\omega^2}{q} \qquad (5.1)$$

For $\Omega^2 > 0$ cases, the modified gyrofrequency increases with the

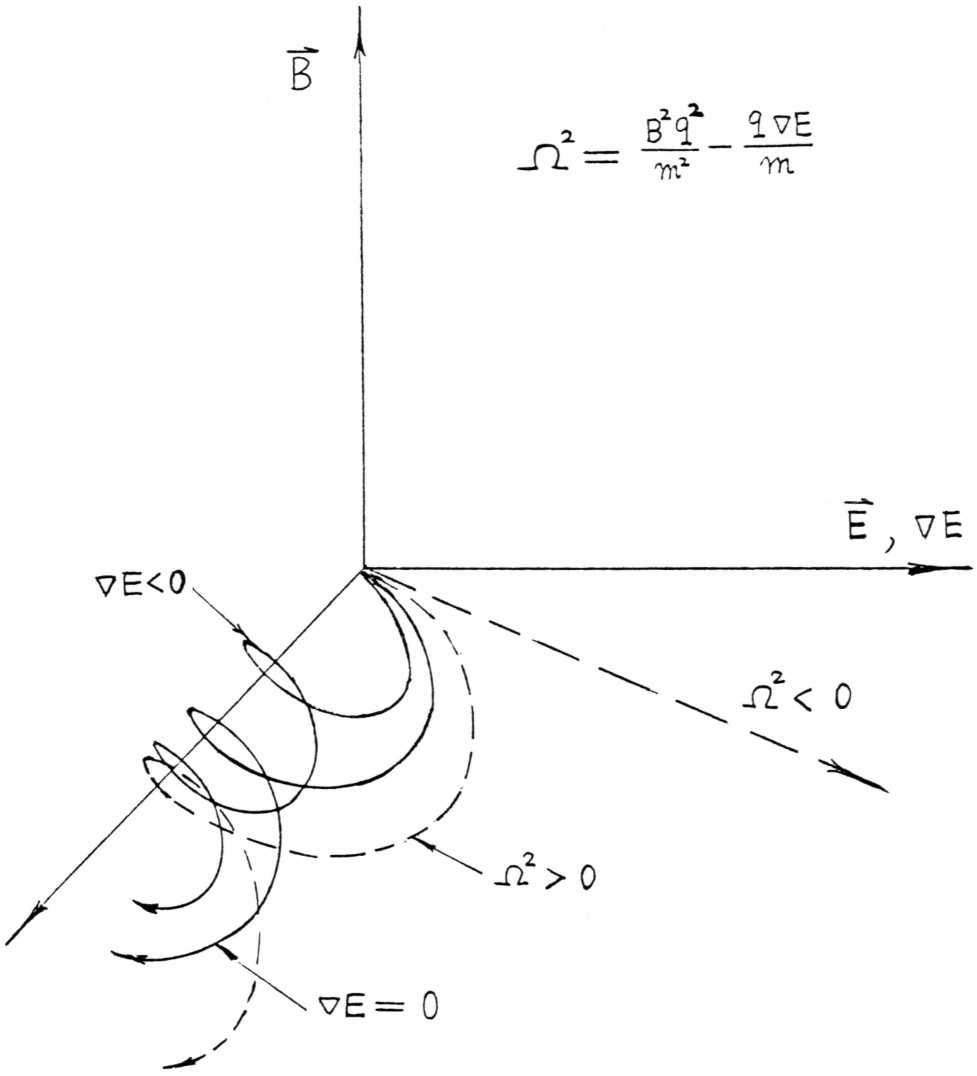

Figure 5.1 Illustration of movement of positively charged particle in crossed $\vec{E}$ and $\vec{B}$ fields in which ∇E exists parallel to $\vec{E}$.

decrease of ∇E; and when $\nabla E = 0$, $\Omega = \omega$. The amplitude of the oscillation in $\vec{E}$ direction decreases with the increase of Ω.

For the V-shaped field model of equation (3.1), when A = 0, it gives a perpendicular electric field in the x direction,

$$E(x) = -\frac{2\phi_o}{L_x^2} x\, e^{-x^2/L_x^2} \tag{5.2}$$

and

$$\nabla E(x) = \frac{2\phi_o}{L_x^2}\left(\frac{2x^2}{L_x^2} - 1\right) e^{-x^2/L_x^2} \tag{5.3}$$

By defining

$$f(x) = \frac{2x}{L_x} e^{-x^2/L_x^2} \tag{5.4}$$

and

$$g(x) = 2\left(\frac{2x^2}{L_x^2} - 1\right) e^{-x^2/L_x^2} \tag{5.5}$$

The equations (5.2), (5.3) can be written

$$E(x) = -\frac{\phi_o}{L_x} f(x) \tag{5.6}$$

and

$$\nabla E(x) = \frac{\phi_o}{L_x^2} g(x) \tag{5.7}$$

The relations of $f(x) - x/L_x$, $g(x) - x/L_x$ are shown in Figure 5.2. The function $f(x)$ attains its maximum value, $f(x)\,|_{max} = \sqrt{2}\, e^{-1/2} \approx 0.858$, at the position $x/L_x = \frac{1}{\sqrt{2}}$, or $x \approx 0.71\, L_x$. The function $g(x)$ attains its maximum value $g(x)\,|_{max} = 4\, e^{-3/2} \approx 0.9$, at the position $x/L_x = (\frac{3}{2})^{1/2}$, or $x \approx 1.22\, L_x$.

We define the characteristic gyroradius ρ_i as the gyroradius of a particle (q,m) of kinetic energy $q\phi_o$ moving with pitch angle 90^o in the magnetic field $\vec{B}$,

$$\rho_i = \frac{mv}{qB} = \left(\frac{2m\phi_o}{q}\right)^{1/2} /B \tag{5.8}$$

Comparing the maximum value of $\nabla E(x)$ of equation (5.7) and the critical value of (5.1), the scale value L_x corresponding to the critical value ∇E is

$$L_{x,max} = \sqrt{2}\, e^{-3/4}\, \rho_i \approx 0.668\, \rho_i \tag{5.9}$$

The $\nabla E(x)$ given by equation (3.7) is not a constant, in fact the correct value of $L_{x,max}$ should be a little larger than that given by equation (5.9). For average,

$$L_{x,max} \approx 0.75\, \rho_i \tag{5.10}$$

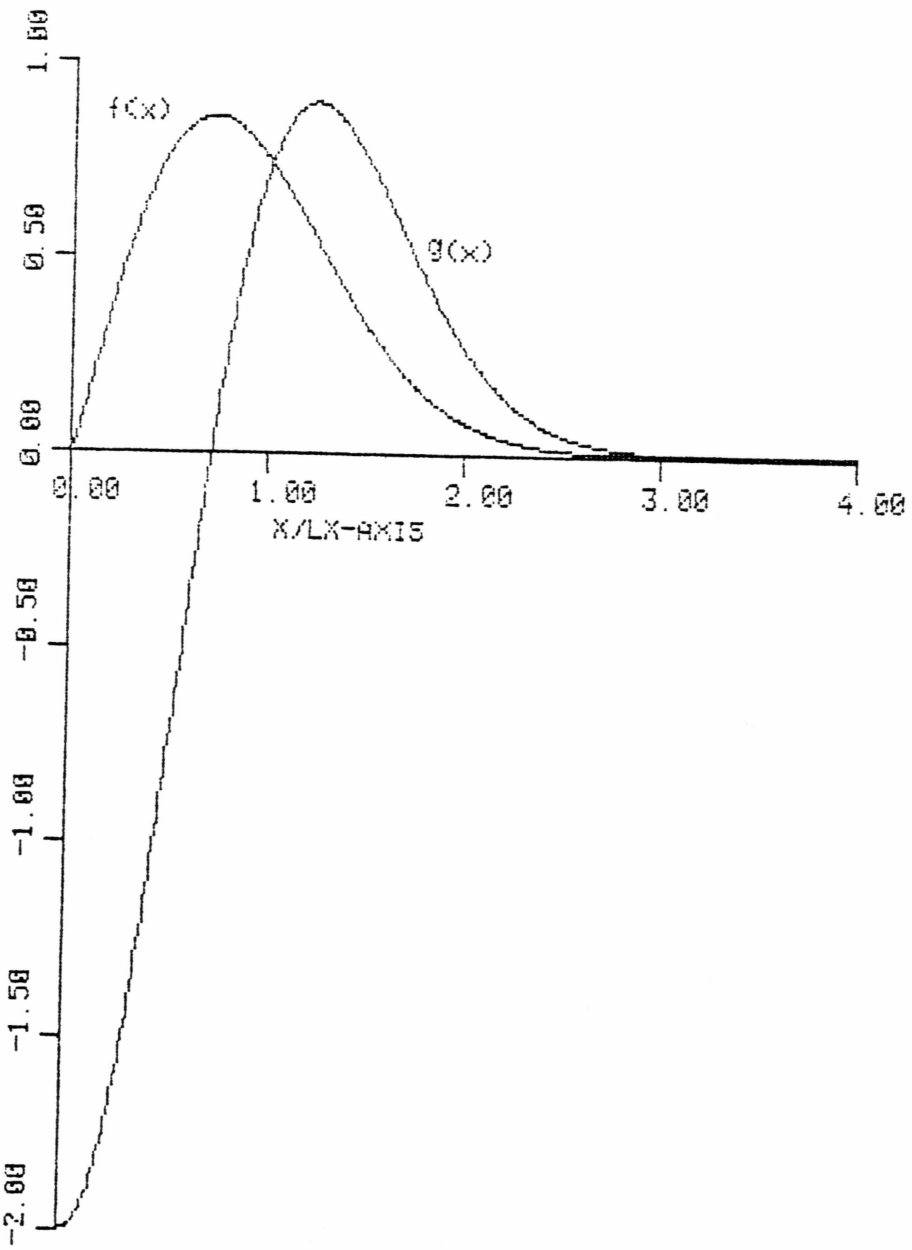

Figure 5.2 Relations of $f(x/L_x) - x/L_x$, $g(x/L_x) - x/L_x$.

Because ρ_i is proportional to the root of the particle mass, value $L_{x,max}$ for O^+ will be 4 times of that for H^+, assuming the case that ϕ_o, $\vec{B}$ are the same. The phenomenon of continuous acceleration in the electric field becomes possible only when $L_x < L_{x,max}$, and only in those regions where ∇E satisfies the critical condition.

For example, ϕ_o = 8 Kv, we get $\rho^* = 4$, and $L^*_{x,max} = 3.0$.

We are more interested in the following question: For a given potential field of equation (5.2), what is the maximum energization region of charged particles? The trajectory study also points out that there exists a critical value of x^*_{max}, when $x^* > x^*_{max}$, the particle can only oscillate with a small amplitude, i.e., the particle cannot get significant kinetic energy gain; while $x^* \lesssim x^*_{max}$, the particle will keep accelerating in the x^* direction in the first period of motion, even the electric field there is quite weak, a large kinetic energy gain can be expected. By investigating the curves given in Figure 5.2, we know, when $\nabla E(x) > \frac{qB^2}{m}$, the particle keeps acceleration in $\vec{E}$ direction and drifts simultaneously in the y^* direction; when $\nabla E(x) \lesssim \frac{qB^2}{m}$, the particle begins to gyrate.

It is obvious that $\vec{E}(x)$ attains its maximum value when $\nabla E = 0$. The effect of $\nabla E(x) < 0$, decreases the gyroradius. Because of the relatively larger electric field around the position of $\nabla E = 0$ and the inertia of the pre-accelerated particle, however,

usually the particle can gyrate across the $x^* = 0$ plane, and attain the maximum kinetic energy there. An example can be seen in Figure 4.1.

For $\phi_o = 8$ KV, $L^*_x = 1.5$, the critical value x^*_{max} derived by comparing the value $\nabla E(x) = \frac{qB^2}{m}$ and the corresponding value from the Figure 5.2, is $\sim 2\ L^*_x$. This value is obtained under the assumption of constant ∇E. The more accurate value for the potential we consider is,

$$x^*_{max} \approx 2.2\ L_x = 3.3 \qquad (5.11)$$

For proton, $x^*_{max} \approx 1780$ m. And in the same potential field, for O^+ ion, the value is about 2400 m.

(2) In V-shaped potential case, the gradient of the perpendicular electric field not only has component in the direction of electric field, but also has component in parallel direction, i.e., in the direction of magnetic field $\vec{B}$. For convenience, we consider uniform $\vec{B}$ in the z direction, electric field $\vec{E}(y,z)$ in the y direction, and the components of gradient ∇E are constant in the y and z direction, respectively. The situation is shown in Figure 5.3.

First we assume the component of gradient $\vec{E}$ only exists in the z direction, i.e., $(\nabla E)_y = 0$. Assume $\vec{V} = (u,v,w)$, and (u_1,v_1,w_1) are the components of velocity at time t= 0 at point (0,0,0).

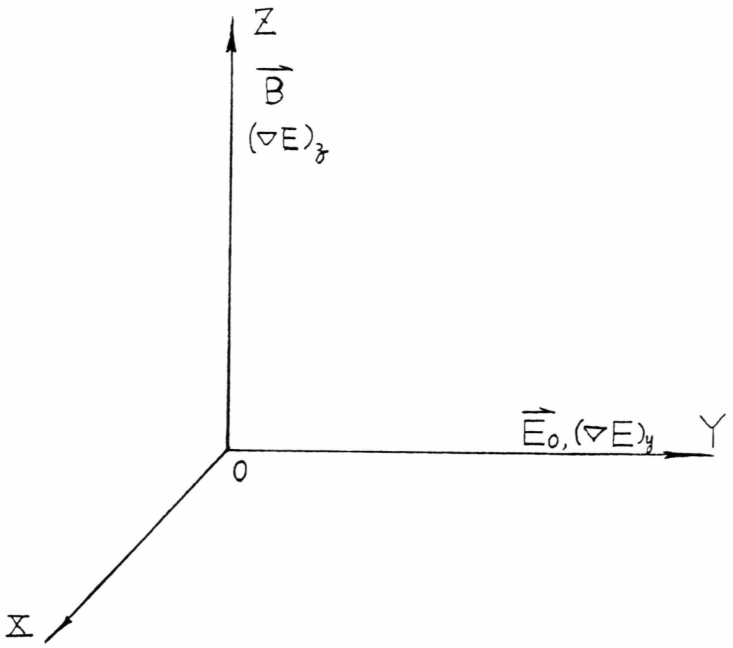

Figure 5.3 Illustration of crossed $\vec{E}$ and $\vec{B}$ fields in which ∇E exists both in the direction parallel to $\vec{E}_o$ and in the direction parallel to $\vec{B}$.

$$\vec{E} = \vec{E}_o + (\nabla E) \cdot z \tag{5.12}$$

The equation of motion is

$$m \frac{d\vec{v}}{dt} = q \left[E_o + (\nabla E) \cdot z\right] \hat{y} + q \vec{V} \times \vec{B} \tag{5.13}$$

In a frame of coordinates given by $X = x - \frac{E_o}{B}t$, $Y = y$, $Z = z$, the equation of motion yields

$$\ddot{X} = \frac{qB}{m} \dot{Y}$$

$$\ddot{Y} = -\frac{qB}{m} \dot{X} + \frac{q\nabla E}{m} Z \tag{5.14}$$

$$Z = w_1 t$$

It follows that

$$\ddot{Y} + \omega^2 Y = \frac{q\nabla E}{m} w_1 t - \omega(u_1 - \frac{E_o}{B}) \tag{5.15}$$

where $\omega = \frac{qB}{m}$.

The solution of equations (5.12) in the original (x,y,z) system becomes

$$u = (u_1 - \frac{E_o}{B}) \cos \omega t + (v_1 - \frac{w_1 \nabla E}{\omega B}) \sin \omega t + \frac{E_o}{B} + \frac{w_1 \nabla E}{B} t \tag{5.16a}$$

$$v = -\left(u_1 - \frac{E_o}{B}\right) \sin \omega t + \left(v_1 - \frac{w_1 \nabla E}{\omega B}\right) \cos \omega t + \frac{w_1 \nabla E}{\omega B} \tag{5.16b}$$

$$w = w_1 \tag{5.16c}$$

together with

$$x = \frac{1}{\omega}\left(u_1 - \frac{E_o}{B}\right) \sin \omega t + \left(\frac{v_1}{\omega} - \frac{w_1 \nabla E}{\omega^2 B}\right)(1 - \cos \omega t) + \frac{E_o}{B} t + \frac{w_1 \nabla E}{2B} t^2 \tag{5.17a}$$

$$y = -\frac{1}{\omega}\left(u_1 - \frac{E_o}{B}\right)(1 - \cos \omega t) + \left(\frac{v_1}{\omega} - \frac{w_1 \nabla E}{\omega^2 B}\right) \sin \omega t + \frac{w_1 \nabla E}{\omega B} t \tag{5.17b}$$

$$z = w_1 t \tag{5.17c}$$

Besides those gyrational terms of frequency ω, which can be expected directly from equation (5.15), it is interesting to note the drift term appearing in equation (5.16b). The charged particle drifts in the direction of the perpendicular electric field with a velocity $\frac{w_1 \nabla E}{\omega B}$. This term will be important when ∇E and w_1 are sufficiently large. The displacement in perpendicular direction is one way of the energy change from the potential to the kinetic in many cases. When $\nabla E = 0$, equations (5.16) and (5.17) reduce to the well-known forms of the charged particle motion in the crossed constant $\vec{E}$ and $\vec{B}$ fields.

(3) Now we consider a more general case that $(\nabla E)y$ does exist. This situation is related to the work done by Cole (1976) and the work done above.

$$\vec{E} = \vec{E}_o + \hat{y}\,((\nabla E)_y \cdot y + (\nabla E)_z \cdot z) \tag{5.18}$$

The equation of motion is

$$m\frac{d\vec{v}}{dt} = q\left[\vec{E}_o + \hat{y}\,((\nabla E)_y \cdot y + (\nabla E)_z \cdot z)\right] + q\,\vec{V} \times \vec{B} \tag{5.19}$$

Similarly, let $X = x - \frac{E_o}{B}t$, $Y = y$, $Z = z$, we obtain

$$\ddot{X} = \frac{qB}{m}\dot{Y}$$

$$\ddot{Y} = -\frac{qB}{m}\dot{X} + \frac{q(\nabla E)_y}{m}Y + \frac{q(\nabla E)_z}{m}Z \tag{5.20}$$

$$Z = w_1 t$$

It follows that

$$\ddot{Y} + (\omega^2 - \frac{q(\nabla E)_y}{m})\,Y = \frac{q(\nabla E)_z}{m}w_1 t - \omega(u_1 - \frac{E_o}{B}) \tag{5.21}$$

Case I

$$\omega^2 - \frac{q(\nabla E)_y}{m} > 0 \tag{5.22}$$

Let

$$\Omega^2 = \omega^2 - \frac{q(\nabla E)_y}{m} \tag{5.23}$$

The solution of equation (5.20) in the original (x,y,z) system is

$$u = \frac{\omega^2}{\Omega^2}(u_1 - \frac{E_o}{B}) \cos \Omega t + \frac{\omega}{\Omega}(v_1 - \frac{qw_1(\nabla E)_z}{m\Omega^2}) \sin \Omega t + u_1 - \frac{\omega^2}{\Omega^2}(u_1 - \frac{E_o}{B}) +$$

$$\frac{q\omega w_1(\nabla E)_z}{m\Omega^2} t \tag{5.24a}$$

$$v = -\frac{\omega}{\Omega}(u_1 - \frac{E_o}{B}) \sin \Omega t + (v_1 - \frac{qw_1(\nabla E)_z}{m\Omega^2}) \cos \Omega t + \frac{q(\nabla E)_z w_1}{m\Omega^2} \tag{5.24b}$$

$$w = w_1 \tag{5.24c}$$

together with

$$x = \frac{\omega^2}{\Omega^3}(u_1 - \frac{E_o}{B}) \sin \Omega t + \frac{\omega}{\Omega^2}(v_1 - \frac{qw_1(\nabla E)_z}{m\Omega^2})(1 - \cos \Omega t) +$$

$$(u_1 - \frac{\omega^2}{\Omega^2}(u_1 - \frac{E_o}{B}))t + \frac{q\omega w_1(\nabla E)_z}{2m\Omega^2} t^2 \tag{5.25a}$$

$$y = -\frac{\omega}{\Omega^2}(u_1 - \frac{E_o}{B})(1 - \cos \Omega t) + (\frac{v_1}{\Omega} - \frac{qw_1(\nabla E)_z}{m\Omega^3}) \sin \Omega t +$$

$$\frac{qw_1(\nabla E)_z}{m\Omega^2}\, t \tag{5.25b}$$

$$z = w_1 t \tag{5.25c}$$

The modified frequency of the oscillation is Ω. The drift velocity along the ox axis is

$$v_D = \frac{\omega^2 E_o}{\Omega^2 B} + u_1 \left(1 - \frac{\omega^2}{\Omega^2}\right) + \frac{q\omega w_1(\nabla E)_z}{m\Omega^2}\, t \tag{5.26}$$

When $(\nabla E)_y = 0$, $(\nabla E)_z = 0$, it reduces to the well-known term $\frac{E_o}{B}$. It is notable in equation (5.24b), the term of drift velocity in the direction of electric field,

$$v_d = \frac{qW_1(\nabla E)_z}{m\Omega^2} \tag{5.27}$$

when Ω decreases, or $(\nabla E)_y$ approaches the critical value $\frac{qB^2}{m}$, this drift velocity becomes large.

Case II

$$\omega^2 - \frac{q(\nabla E)_y}{m} < 0 \tag{5.28}$$

Let

$$\phi^2 = \frac{q(\nabla E)_y}{m} - \omega^2 \tag{5.29}$$

The solution of equation (5.20) in the original system (x,y,z) is

$$u = \frac{\omega}{\phi}\left(v_1 + \frac{qw_1(\nabla E)_z}{m\phi^2}\right) sh\phi t - \frac{\omega^2}{\phi^2}\left(u_1 - \frac{E_o}{B}\right)ch\phi t + u_1 + \frac{\omega^2}{\phi^2}\left(u_1 - \frac{E_o}{B}\right) - \frac{q\omega w_1(\nabla E)_z}{m\phi^2} t \qquad (5.30a)$$

$$v = -\frac{\omega}{\phi}\left(u_1 - \frac{E_o}{B}\right) sh\phi t + \left(v_1 + \frac{qw_1(\nabla E)_z}{m\phi^2}\right)ch\phi t - \frac{qw_1(\nabla E)_z}{m\phi^2} \qquad (5.30b)$$

$$w = w_1 \qquad (5.30c)$$

The particle drifts in the direction of $\vec{E} \times \vec{B}$, and also accelerated in the direction of $\vec{E}$. The drift term in the direction of $\vec{E}_o$ that appears in equation (5.30b), is with negative sign. When $(\nabla E)_y = 0$, equations (5.30) reduce to equations (8.16); when $\nabla E = 0$, equations (5.30) reduce to the well-known results, $\phi = \omega$.

For more general cases, there exists parallel electric field, i.e., velocity w_1 is not constant. And also ∇E is not constant in V-shaped potential. However, the solution in the simplized cases, does help in understanding the energization process in V-shaped or other kind of two dimensional potentials.

In V-shaped potential, the particles are accelerated both in the perpendicular and in the parallel direction. At sufficiently high altitudes, the potential reduces to the form of equation (5.2). Due to the drift motion in the direction of perpendicular electric field, the acceleration region will be a little larger than

that given by equation (5.11). The patterns of this drift motion can be seen in the trajectories of the numerical study.

(4) From the above study, we can generalize the particle motion in a V-shaped potential as follows:

When the transverse electric field scale $L_x < 0.75\ \rho_i$, the continuous acceleration in the direction of the transverse electric field will become possible for those charged particles, which can reach the region which satisfies the critical condition, $\nabla E > \frac{qB^2}{m}$. Those particles can be expected to attain large kinetic energy gain, large pitch angle and large amplitudes of oscillations in the direction of the transverse electric field. The drift motion in the direction of the electric field, see equation (5.27), can be seen at the first period of energization process. An example can be seen in Figure 4.3. For those particles that cannot reach the region, in which the critical electric field gradient value could be satisfied, no continuous acceleration in the direction of the transverse electric field will occur. The particles will gyrate, accelerate in the parallel direction, drift in the $\vec{E} \times \vec{B}$ direction, and drift in the direction of the transverse electric field. From equation (5.27), $v_d \propto (\nabla E)z$, this drift velocity will vanish as $(\nabla E)z \to 0$, when $z \to \infty$. Finally, those particles will oscillate with small amplitudes. Figure 4.2 shows an example for this case.

When the transverse electric field scale $L_x > 0.75\ \rho_i$, the critical condition examined by Cole (1976) will not be satisfied, the effect of the motion $\vec{v}_d$ is important for the final results.

This drift term increases in the first period of the energization process, because w_1 and $(\nabla E)_z$ increase then. This drift velocity will decrease and vanish when z is sufficient large because $(\nabla E)_z$ decreases and vanishes then. The result is, particle oscillates with small amplitude, i.e., energy gain in the direction of transverse electric field is small. The transverse energy gain will quite depend on the drift term in $\vec{E} \times \vec{B}$ direction, see equation (5.26). An example of the trajectory can be seen in Figure 4.7.

6. Summary of Ion Conic and Beam Formation

It is clear that when the transverse scale of the electric field $L_x >> \rho_i$, the upward flowing ions move along the magnetic field lines with a small transverse velocity due to the $\vec{E} \times \vec{B}$ drift; their small oscillation can be neglected. In this case the ion beams are formed. The energy-latitudinal spectrogram for these ion beams has a shape similar to the potential drop function $\Delta\Phi(x)$, which is determined by the potential structure.

The trajectory study of this thesis is to elucidate dynamic behaviors of ions in the V-shaped or S-shaped DC electric field associated with the auroral arc. From section 4 and section 5, we have already seen that the acceleration of the ions in the field models with transverse scale $L_x \lesssim \rho_i$ will naturally lead to angular distributions of conic, of which the phenomena are frequently observed in the polar region. The different pitch angle and kinetic energy distributions of the upward flowing ions are the results of

the acceleration in the electric field with different scales and characteristic parameters of the potential structure.

For a V-shaped potential with $L_x \sim \rho_i$ or a few times of ρ_i, an example seen in case (D) of section 4.2, the ions have small pitch angle value at the central part. As a result, an ion beam is formed. Beyond this part, the pitch angle of the upward ions is increasing and larger than 10^o, so that the conic could be observed over there. One distinct characteristic of this ion motion is that the transverse kinetic energy is mostly due to the drift in $\vec{E} \times \vec{B}$ direction. This means that the perpendicular motion of the ions is in the positive or negative y-direction, respectively, for $x > 0$ or $x < 0$ hemi-space. The direction of motion is nearly perpendicular to the x-axis. The characteristic features of this drift of the upward moving test particles are in agreement with the observed, fast $\vec{E} \times \vec{B}$ drift in auroral structures (Lennartsson, 1980).

For the $L_x \lesssim 0.7\ \rho_i$ case, most of the acceleration in the V-shaped potential will produce the conic, though in the pure V-shaped case we might see an intense ion flux with pitch angles smaller than 10^o in the central part. An example of this case can be seen in Figure 4.4, where the $\alpha - x_o^*$ curve shows that ions originated from $|x_o^*| \lesssim 0.75$ will have final pitch angles smaller than 10^o. The oscillation in the x direction is usually considerably large, especially for the common cases of $A < 1$.

The physical meaning of the parameter A of the V-shaped potential function of equation (3.1), also the parameter γ of the S-

shaped potential function of equation (3.5), can be seen from the equipotential structure of the field models. The large pitch angle ($\sim 90^{o}$) distribution, i.e. the "pancake" phenomena, can be explained as the results of the acceleration in V-shaped potentials, which have the quasi-parallel equipotential structure, or $A \to 0$ for our field model. The peak value of the pitch angle distribution decreases gradually with the increase of A. The extreme case is the pure V-shaped corresponding to $A = 1$. The studies of the variation of the pitch angle and kinetic energy gain with the different A value, do give us information about what might be the results of the acceleration in an electric potential of which the parallel electric field component dominates or the perpendicular component dominates. This study can be applied to other cases, there exists both parallel and perpendicular electric fields but not exactly the V-shaped or S-shaped.

The pancake-like pitch-angle distributions are often observed in a low altitude ($\sim$ 400 - 600 km). This phemomenon could be the result of the ion acceleration in the region III of a V-shaped potential, see Figure 3.3, where the potential has a parallel equipotential or probably a quasi-parallel equipotential structure. When these pre-accelerated ions reach the region I or the region II, they will be accelerated both in the parallel and in the perpendicular direction. That leads to conic at high altitude, of which the peak value is less than 90^{o}. For a test particle pre-accelerated to 0.4 keV, assuming its pitch angle 85^{o}, phase angle

80^{o} (y^{*} axis is zero phase, anti-clockwise is positive), $x_{o}^{*} = 2.0$, when it reaches the $z^{*} = 0$ plane, the final value due to the acceleration in region I and II are, $E_{k} \sim 4.2 - 6.6$ keV, and $\alpha \sim 41^{o} - 53^{o}$.

The results of statistical study of the behavior of the observed upward flowing O^{+} and H^{+} are used to infer that the O^{+} ions receive higher energy and have wider pitch angle widths than H^{+} ions (Sharp, 1980). This relative O^{+} and H^{+} energy distributions and angular distributions are considered to be consistent with a mass dependent transverse acceleration mechanism which preferentially acts on the O^{+} ions. Several mechanisms with these characteristics have been proposed by Lysak et al. (1980) involving resonant wave-particle interactions, and Lennartsson (1980) involving fluctuating or small-scale transverse electric fields, et al.

In Section 4, we have already seen that the O^{+} ions will have distinctly larger pitch angles, larger kinetic energy gain and larger acceleration region than H^{+} ions in the V-shaped DC electric potential in which A is not close to 1.0. Therefore, we believe that this characteristic of the observed O^{+} and H^{+} can be explained as a direct result of the acceleration in the V-potential double layers. And we can also come to this conclusion that most cases in which O^{+} and H^{+} ions are observed, are accelerated in a potential pattern like that shown in Figure 3.3 ($A < 1$).

It should be noted that the acceleration in a V-shaped potential will lead to a non-uniform latitudinal distribution in

pitch angle and kinetic energy. The particles attain the maximum kinetic energies and the maximum pitch angles at their closest positions to the $x^* = 0$ plane. The intense energetic ion flux is formed around the $x^* = 0$ plane in most cases. The observed ion conic distribution cannot be identified with acceleration in narrow V-potentials yet, because the transit time of a satellite through the potentials is much less than the time it takes to observe the conics. A more detailed observation is needed to make clear the pitch angle-latitudinal relation and the energy-latitudinal relation of upward flowing ions. This will be helpful for our understanding of the nature of the energization process of the ions in the electric field existing in the discrete auroral arcs and the formation of ion conics.

The ion acceleration process in the S-shaped potential is very similar to that in the V-shaped. For the $L_x \lesssim \rho_i$ case, the acceleration leads to a ion conic distribution.

7. Conclusion

The results of this study can be summarized as follows:

(1) The ion trajectories in the two-dimensional V-shaped and S-shaped auroral potential structures can be described by five types of motion patterns:

(a) Continuous acceleration in the direction of transverse electric

field when the component of ∇E in this direction is larger than the critical value; this acceleration will lead to a large amplitude of oscillation.

(b) Drift motion in the direction of the transverse electric field when the gradient ∇E of the transverse electric field has a component parallel to the magnetic field; in a V-shaped potential, this component is always > 0, and it approaches to zero, when $z \to \infty$; the velocity of this drift motion will increase, then decrease, and finally vanish with the increase of the altitude z; the drift motion makes the ions moving towards the central part of the V-shaped potential.

(c) Drift motion in the $\vec{E} \times \vec{B}$ direction.

(d) Gyrational motion.

(e) Acceleration in the parallel direction.

(2) The ion acceleration in a V-shaped or S-shaped auroral potential with a transverse scale length $L_x \lesssim \rho_i$, can lead to a conic distribution. Different potential structures correspond to different angular and energy distribution of the upward flowing ions. The results of this study support the idea that the conic distribution of upward flowing ions can be produced by the

perpendicular ion acceleration in the V-shaped and S-shaped quasi-static auroral potential.

(3) Due to the acceleration in a V-shaped or S-shaped potential, the O^+ ions usually have larger kinetic energy gain and a wider acceleration region than H^+. In a thin potential structure or $L_x \lesssim 0.7\ \rho_i$ (scaling in H^+ gyroradius), the maximum kinetic energy should be the same for O^+ and for H^+, this is also true for O^+ and H^+ ions at the central part of the V-shaped structure of large scale L_x. These results are in agreement with the observations reported by Collins et al. (1980).

REFERENCES

Block, L. P., Acceleration of aurora particles by electric double layers, in Earth's Magnetospheric Processes, edited by B. M. McCormac, 258 pp., Reinhold, New York, 1972.

Cattell, C. A., R. L. Lysak, R. B. Torbert, and F. S. Mozer, Observations of differences between regions of current flowing into and out of the ionosphere, Geophys. Res. Lett., 6, 621, 1979.

Chiu, Y. T., J. M. Cornwall, Electrostatic model of a quiet auroral arc, J. Geophys. Res., 85, 543, 1980.

Chiu, Y. T., A. L. Newman, On the structures and mapping of auroral electrostatic potentials, report no. SSL-81(7951)-1, space science laboratory, 1981.

Cladis, J. B., R. D. Sharp, Scale of electric field along magnetic field in an inverted V event, J. Geophys. Res., 84, 6564, 1979.

Cole, K. D., Effects of crossed magnetic and (spatially dependent) electric fields on charged particle motion, Planet. Space Sci., 24, 515, 1976.

Collin, H. L., R. D. Sharp, E. G. Shelley, and R. G. Johnson, Some general characteristics of upflowing ion beams over the aurora zone and their relationship to auroral electrons, submitted to J. Geophys. Res., 1980.

Davis, T. N., Observed characteristics of auroral arcs, Space Sci. Rev., 12, 77, 1978.

Dusenbery, P. B., L. R. Lyons, The generation of ion-conics via quasi-linear diffusion, presented at Chapman Conference on the formation of auroral arcs, 1980.

Fennell, J. F., Auroral particle distribution functions and their relationship to inverted Vs and auroral arcs, to be published in the Proceedings of the Chapman Conference on the formation of auroral arcs, 1980.

Ghielmetti, A. G., R. G. Johnson, R. D. Sharp, and E. G. Shelley, The latitudinal, diurnal, and altitudinal distributions of upward flowing energetic ions of ionospheric origin, Geophys. Res. Lett., 5, 59, 1978.

Gorney, D. J., A Clarke, D. Croley, J. Fennell, J. Luhmann, and P. Mizera, The distribution of ion beams and conics below 8000 km, J. Geophys. Res., 86, 83, 1981.

Gurnett, D. A., Electric field and plasma observations in the magnetosphere, in Critical Problems of Magnetospheric Physics, E. R. Dyer, ed., National Academy of Sciences, 1972.

Kan, J. R., Energization of auroral electrons by electrostatic shock waves, J. Geophys. Res., 80, 2089, 1975.

Kan, J. R., L. C. Lee, and S.-I. Akasofu, Two-dimensional potential double layers and discrete auroras, J. Geophys. Res., 84, 4305, 1979.

Lennartsson, W., On the consequences of the interaction between the auroral plasma and the geomagnetic field, Planet. Space Sci., 28, 135, 1980.

Lichtenberg, A., Phase Space Dynamics of Particles, p. 56, John Wiley, New York, 1969.

Lin, C. S. and R. A. Hoffman, Characteristics of the inverted V event, J. Geophys. Res., 84, 1514, 1969.

Lysak, R. L., M. K. Hudson, and M. Temerin, Ion heating by strong electrostatic ion cyclotron turbulence, J. Geophys. Res., 85, 678, 1980.

Maggs, J. E., and T. N. Davis, Measurements of the thicknesses of auroral structures, Planet. Space Sci., 16, 205, 1968.

Mizera, P. F. and J. F. Fennell, Signatures of electric fields from high and low latitude particle distributions, Geophys. Res. Lett., 4, 311, 1977.

Mizera, P. F., J. F. Fennel, D. R. Croley, Jr., and D. J. Gorney, Charged particle distributions and electric field measurements from S3-3, submitted to J. Geophys. Res., 1981.

Mozer, F. S., C. W. Carlson, M. K. Hudson, R. B. Torbert, B. Parady, J. Yatteau, and M. C. Kelley, Observations of paired electrostatic shocks in the polar magnetosphere, Phys. Rev. Lett., 38, 292, 1977.

Mozer, F. S., C. A. Cattell, M. K. Hudson, R. L. Lysak, M. Temerin, and R. B. Torbert, Satellite measurements and theories of low altitude auroral particle acceleration, Space Science Laboratory, 1980.

Okuda, H., M. Ashour-Abdally, Formation of a conical distribution and intense ion heating in the presence of hydrogen cyclotron waves, Geophys. Res. Lett., 8, 811, 1981.

Sharp, R. D., Positive ion accelration in the 1 R_E altitude range, proceedings of the Chapman Conference on the Formation of Auroral Arcs, 1980.

Sharp, R. D., R. G. Johnson, and E. G. Shelley, Observation of an ionospheric acceleration mechanism producing energetic (keV) ions primarily normal to the geomagnetic field direction, J. Geophys. Res., 82, 3324, 1977.

Sharp, R. D., R. G. Johnson, and E. G. Shelley, Energetic particle measurements from within ionospheric structures responsible for auroral acceleration process, J. Geophys. Res., 84, 480, 1979.

Shelley, E. G., R. D. Sharp, and R. G. Johnson, Satellite observations of an ionospheric acceleration mechanism, Geophys. Res. Lett., 3, 654, 1976.

Swift, D. W., On the formation of auroral arcs and acceleration of auroral electrons, J. Geophys. Res., 80, 2096, 1975.

Swift, D. W., An equipotential model for aurora arcs, J. Geophys. Res., 81, 3935, 1976.

Swift, D. W., An equipotential model for auroral arcs: the theory of two-dimensional laminar electrostatic shocks, J. Geophys. Res., 84, 6427, 1979.

Swift, D. W., H. C. Stenbaek-Nielsen, and T. J. Hallinan, An equipotential model for auroral arcs, J. Geophys. Res., 81, 3931, 1976.

Wagner, J. S., J. R. Kan, and S.-I. Akasofu, Particle dynamics in the plasma sheet, J. Geophys. Res., 84, 891, 1979.

Whalen, B. A., Low altitude acceleration of ionospheric ions, Geophys. Res. Lett., 5, 55, 1978.